Dynamics of Agulhas Retroflection and Ring Formation in a Numerical Model. Part I: The Vorticity Balance

DOUGLAS B. BOUDRA AND ERIC P. CHASSIGNET

Rosenstiel School of Marine and Atmospheric Science, University of Miami, Miami, Florida

(Manuscript received 30 December 1986, in final form 7 July 1987)

ABSTRACT

The Agulhas retroflection region of the wind-driven idealized South Atlantic–Indian Ocean model described by DeRuijter and Boudra is analyzed in detail. Here, in Part I, the physical mechanisms of the model retroflection are elucidated through illustration of the Agulhas' vorticity balance among various experiments. In Part II, the ring formation process is described in terms of its vertical structure and the associated energy conversions.

A one-layer model demonstration shows that both inertia and internal friction may account for a partial retroflection where a linear, weakly viscous system has none. In the nonlinear, weakly viscous one-layer model, the retroflection is accomplished through a free inertial boundary layer, as suggested originally by De Ruijter. When stratification is introduced and baroclinicity increased, using the Bleck and Boudra quasi-isopycnic coordinate model with 2 or 3 layers, the stretching term exerts an increasing influence. With 40-km resolution, terms included so that the numerical model conserves potential vorticity become important as well. Both encourage retroflection of the fluid separating from Africa's tip. When grid spacing is halved, the importance of the extra conserving terms diminishes and the stretching term exerts an even greater influence. The importance of a substantial viscous stress curl along the coast of Africa, as provided by the no-slip condition, is illustrated through comparison with a slippery Africa experiment.

Finally, an experiment with a more realistic South African coastal geometry, giving a more realistic order of importance to βv in the separating Agulhas, is described. It is shown that the retroflection is still strong but that the associated recirculation is less intense. An interesting new aspect of the retroflection is the separation of the mean current core from the coast a few hundred kilometers upstream from the tip. The planetary vorticity advection term plays a smaller role along the coast. Viscous effects on the coastal side of the current are still strong, however, and are balanced primarily by stretching and relative vorticity advection. As the mean current passes Africa's tip, the sink of positive vorticity produced in the stretching and planetary vorticity advection terms is left behind, and the Agulhas turns eastward. These results support the notion, advanced by De Ruijter and Boudra, that the change in the vorticity balance at separation leads to the model retroflection, and they point to the increasing importance of the divergent component of flow in the vorticity balance as more realism is introduced.

1. Introduction

One of the most intriguing features in world ocean circulation is the retroflection of the Agulhas Current south of Africa, and an important phenomena associated with it is ring formation at its western edge. The Agulhas constitutes the primary boundary current of the southwestern Indian Ocean, and as it separates from the southern tip of Africa in a southerly or southwesterly direction, the major part of it retroflects, returning eastward to rejoin the subtropical gyre. Several times a year, in retroflecting, the current cuts itself off and a lense of warm, salty Indian Ocean water (called an Agulhas ring) is formed. Recently, such an event was observed on a hydrographic data gathering cruise and reported by Lutjeharms and Gordon (1987). In assessing the characteristics of this ring and ascribing them to most Agulhas rings, Olson and Evans (1986) suggest that Agulhas rings are the most energetic in the world ocean. In addition, as they drift westward or northwestward, the rings can have an important impact on the kinetic and potential energy budgets of the South Atlantic Ocean.

Several approaches have been used to physically explain the retroflection. Darbyshire (1972) and Lutjeharms and van Balleygooyen (1984) studied the topographic control of a free inertial jet as described by Warren (1963) and by Niiler and Robinson (1967). Application to the Agulhas retroflection showed that small changes in bottom velocity in their models greatly changes the calculated path of the Agulhas after separation. In addition, it was found that the magnitude of the volume transport of the jet is an important factor in determining whether the current penetrates westward or stages an early retroflection. De Ruijter (1982) showed that a linear Munk-type model of wind-driven ocean circulation cannot produce a significant eastward

Corresponding author address: Dr. Douglas B. Boudra, Rosenstiel School of Marine & Atmospheric Science, 4600 Rickenbacker Causeway, Miami, Florida 33149-1098.

turning of the Agulhas south of Africa, even with a fairly realistic shape for the continent. In a shallow, one-layer, inertial–frictional extension of the linear model, inertia carries the fluid parcels far enough southward to partially close the subtropical gyre.

Ou and de Ruijter (1986) obtained a retroflection when they applied their model of inertial boundary current separation to the Agulhas Current. Their reduced gravity model incorporated inertia, the β-effect, and coastline curvature. The separation occurred when the interface between the moving and motionless layers outcropped. This position was upstream of where it would be for a straight coast in the case of the convex shape of South Africa. The positions of the separation and retroflection also depended strongly on the volume flux of the current. Their model does not include lateral friction or temporal variability.

De Ruijter and Boudra (1985) and Boudra and de Ruijter (1986) (henceforth referred to as DB and BD, respectively) included temporal variability and friction in addition to inertia and the β-effect in a study of the South Atlantic–Indian Ocean circulation, using first a one-layer simplification of, and then the full quasi-isopycnic coordinate numerical model of Bleck and Boudra (1981). Perhaps overly idealized aspects of their model were the simple rectangular shape for Africa and the small total basin size. In DB and BD, the primary focus was on parameters affecting the exchange of fluid between the two basins. Their model retroflection was explained primarily in terms of the vorticity balance, in which the no-slip African coast and the magnitude of planetary vorticity advection at separation figured prominently. Influence of several other model parameters among their experiments, including internal lateral friction, horizontal resolution, stratification, incorporation of bottom drag, and interaction with the other wind-driven currents helped establish the changes in the vorticity balance at separation as the central cause of retroflection.

In this paper, the retroflection region of the above numerical model is analyzed in detail. In Part I, we focus on the retroflection vorticity balance and how the importance of certain components of the balance changes as the crucial model parameters are varied. In Part II, (Chassignet and Boudra, 1988) we examine the energetics of the experiments, particularly of the retroflection and the eddy detachment process.

Here in Part I, first, a simple one-layer demonstration shows that a substantial retroflection can be established within a purely frictional boundary layer, an inertial–frictional boundary layer, or a primarily inertial boundary layer. The last of these was suggested in de Ruijter's (1982) nonlinear extension of his linear analytical solutions. In our experiments, it is the viscous stress curl, relative vorticity advection, or a combination of the two which balances βv so that a portion of the Agulhas retroflects. Second, it is shown that when stratification is introduced, as in the 2- and 3-layer experiments of BD, two additional factors must be considered in the retroflection vorticity balance: 1) the stretching term, the importance of which increases with the ratio of local variations in layer thickness to the total layer thickness, and 2) terms involving the numerical model's conservation of potential vorticity and potential enstrophy. Like the β-effect, both of these contribute to the strength of the retroflection (the ratio of the transport of retroflected water to that of the Agulhas at separation). The role played by the second factor is smaller when grid resolution is improved since the numerical model better approximates the differential equations, which naturally conserve those properties. In a new, high resolution experiment with more realistic South African geometry, the current core separates a few hundred kilometers upstream of Africa's tip. The Agulhas continues southwestward, however, and near the tip the great part of it still retroflects. In the vorticity balance along the coast, viscous effects are balanced by positive vorticity generation primarily in the relative vorticity advection and stretching terms. As the current passes Africa's tip, the magnitude of the latter decreases and positive vorticity in the retroflection itself is generated by approximately equal components of stretching and planetary vorticity advection. With the introduction of stratification and more realistic geometry, then, the divergent component of the flow becomes a major factor in the retroflection vorticity balance through the stretching term and, indeed, one of the important physical mechanisms of retroflection.

The layout of the paper is as follows. In section 2, we review the model characteristics and give a table of the experiments. The method of analyzing the vorticity balance is presented in section 3. A one-layer model demonstration, including first friction and then inertia is given in section 4. The balance in several of the multilayer experiments of BD is described in section 5. The new experiment with more realistic African geometry is introduced and its vorticity balance discussed in section 6. We summarize the results of our analysis in section 7, and we discuss their significance, while comparing with the Ou and de Ruijter (1986) model, in the concluding section.

2. Description of the model and the experiments

The numerical models used in this study are 1) a one-layer simplification of and 2) the full Bleck and Boudra (1981) quasi-isopycnic coordinate, primitive equation model, referred to hereafter as the BB model. The model has a rigid lid, so that 1) closely approximates a one-layer quasi-geostrophic model. The advantages of the coordinate system of 2) are that vertical resolution is concentrated where it is most needed—in regions of large horizontal density gradients—and the relatively large, numerically required lateral diffusion is along isopycnal surfaces, which are almost

coincident with the preferred mixing surfaces of the ocean. To avoid the numerical difficulty associated with coordinate surface outcropping (zero layer thickness), the quasi-isopycnic coordinate model disallows layers becoming thinner than a certain value (in our case, 40 db), so that fluid is allowed to pass through a layer interface when a thickness less than that minimum is predicted. In such regions, the coordinate loses its isopycnic nature and a thermodynamic equation is included in the model to deal with layer density variations. In the experiments discussed here, due to the choice of stratification and forcing parameters, fluid is rarely exchanged between layers, and, thus, the model may be considered a purely isopycnic coordinate one. Additional details of the model may be found in BB.

DB and BD configured the model in an east–west oriented rectangular basin, illustrated here in Fig. 1, to study the influence of the Agulhas retroflection strength on the South Atlantic–Indian Ocean circulation. The steady wind stress profile is shown at the left of the figure. It is seen that anticyclonic wind forcing extends in each basin from the northern boundary to 280 km north of the southern boundary. The westerly wind curl zero is at this position and the southernmost portion of the basin is forced cyclonically. The lateral boundary conditions are generally no-slip ($u = v = 0$) on meridionally oriented boundaries and free-slip ($v = du/dy = 0$) on zonally oriented boundaries. The exception is the coast of Africa, which is entirely no-slip but for one experiment in which it is free-slip.

The circulation pattern which develops as the model is spun up from rest consists of an elongated subpolar gyre near the southern boundary with a linear Sverdrup transport of approximately 10 Sv (1 Sv $\equiv 10^6$ m^3 s^{-1}) and subtropical gyres in the Atlantic and Indian Ocean sectors with linear interior transports of 30 and 45 Sv, respectively. Placing the wind curl zero 400 km south of the tip of Africa, roughly corresponding to its wintertime climatological mean position (Hellerman and Rosenstein, 1983), allows for interaction of the subtropical gyres, and the amount of exchange is governed by the strength of the retroflection of the Agulhas back into the Indian Ocean after it reaches Africa's tip. As shown by BD, the strength is approximately proportional to the Rossby number of the current at the tip as long as the no-slip condition is specified on Africa. With the free-slip condition the retroflection is essentially nonexistent. In addition, at the boundary between the subtropical gyres and the subpolar gyre is a region of eastward drift, accompanied by a frontal-type feature in the multilayer cases, which may interact with the retroflecting current much as the northern edge of the Antarctic Circumpolar Current interacts with the Agulhas Return Current.

Many of the experiments of focus here were first introduced in DB and BD, but a few new ones have been formulated to clarify some aspects of the vorticity balance, and one to give the β-effect a more realistic importance. The experiments are defined in Table 1, which includes a short description of the retroflection, or lack of it, in each, and indicates where the experiment has been described before, if such is the case.

3. Method of analysis

To develop an equation from which the vorticity balance of the above model may be analyzed, we begin by writing the differential form of the equation of motion for the BB model, with the generalized vertical coordinate denoted by the letter s:

$$\left(\frac{\partial \mathbf{v}}{\partial t}\right)_s = -\frac{\nabla_s \mathbf{v}^2}{2} - (\zeta_s + f)\mathbf{k} \times \mathbf{v} - \left(\dot{s}\frac{\partial p}{\partial s}\right)\frac{\partial \mathbf{v}}{\partial s} - \alpha \nabla_s p - \nabla_s \phi + \alpha \frac{\partial \tau}{\partial z} + A\left(\frac{\partial p}{\partial s}\right)^{-1} \nabla_s \cdot \left(\frac{\partial p}{\partial s}\nabla_s \mathbf{v}\right) \quad (3.1)$$

where A is the lateral viscosity and the other symbols are conventional. Extracting the vertical component from the curl of (3.1) yields the differential form of the relative vorticity equation:

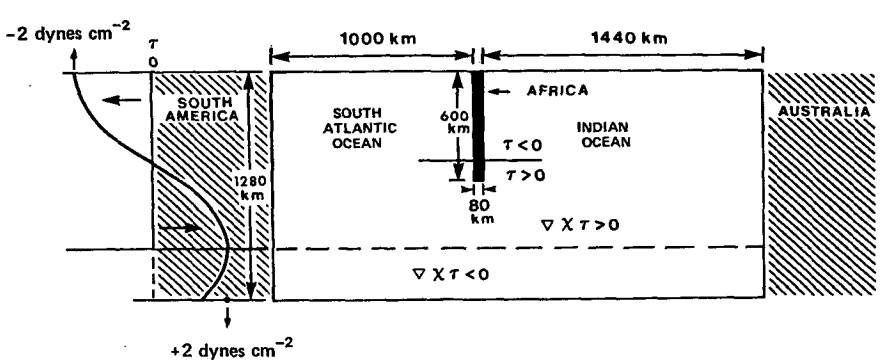

FIG. 1. Geometry of the flat bottom ocean basin used in all the numerical experiments, except E11. The wind stress profile is shown at the left.

TABLE 1. Description of the experiments. Blanks indicate no change from the previous experiment.

Experiment	Number of layers	Thickness of the layers (m)	g' (m s^{-2})	Viscosity (m^2 s^{-1})	Bottom drag coefficient (s^{-1})	Boundary conditions on Africa[1]	Horizontal resolution (km)	Africa's geometry[2]	Description of the upper layer flow pattern of the model retroflection region (where previously described)
LIN1	1	1 000		330		NS	40	A	Linear solution. Small recirculation cell east of Africa. Most of the flow (35 Sv) goes into the Atlantic.
NLIN1									Substantial retroflection extending southwest of the tip of Africa. Approx. 15 Sv leakage into the Atlantic. High temporal variability. (De Ruijter and Boudra, 1985).
LIN2				3 300					Linear solution. Establishment of a retroflection but with 20–25 Sv leakage.
NLIN2									Similar to LIN2. The retroflection is moved south and west of the separation point. Steady solution.
E1	2	1 000 4 000	0.02	330					Similar to NLIN1, but with 25 Sv leakage and less variability. (Boudra and de Ruijter, 1986) (BD).
E2	3	600 700 3 700	0.02 0.005						Similar to E1, but with 15 Sv leakage and the position of the retroflection closer to the separation from Africa. (BD).
E3		300 900 3 800							The current retroflects very soon after it separates from the coast. Small leakage (less than 5 Sv). High eddy energy in the retroflection. (BD).
E8					10^{-7}				Similar to E3, but the circulation is more intense. (BD).
E9						FS			Most of the flow turns westward and then northward along the coast into the Atlantic. 10 Sv recirculation southeast of Africa. (BD).
E10						NS	20		Similar to E3, but with less intense retroflection and a strong downstream meander. (BD).
E11								B	The boundary current is broader with smaller velocities than E10. The retroflection is still strong, but is less intense and there is 5–10 Sv leakage.

[1] NS = No-Slip, FS = Free-Slip.
[2] A = Rectangular (Fig. 1), B = More realistic (Fig. 10).

$$\frac{\partial \zeta_s}{\partial t} = -\mathbf{v}\cdot\nabla_s\zeta_s - \beta v - (\zeta_s + f)\nabla_s\cdot\mathbf{v}$$
(1) (2) (3) (4)
$$- \mathbf{k}\cdot\left[\nabla_s\times\left(\dot{s}\frac{\partial p}{\partial s}\right)\frac{\partial \mathbf{v}}{\partial s}\right] - \mathbf{k}\cdot[\nabla_s\alpha\times\nabla_s p]$$
(5) (6)
$$+ \mathbf{k}\cdot\nabla_s\times\alpha\frac{\partial \tau}{\partial z} + A\mathbf{k}\cdot\left[\nabla_s\times\left(\frac{\partial p}{\partial s}\right)^{-1}\nabla_s\cdot\left(\frac{\partial p}{\partial s}\nabla_s\mathbf{v}\right)\right].$$
(7) (8)
(3.2)

The curl of the first term on the right side of (3.1) vanishes. The curl of the second term on the right of (3.1) has been broken up into terms 2, 3 and 4 in (3.2), denoting relative vorticity advection, planetary vorticity advection, and stretching, respectively. Term 5 is known as the tilting/twisting term, term 6 the solenoidal term, term 7 the wind stress curl, and term 8 the viscous stress curl.

In order to develop an equation corresponding to (3.2) from which the vorticity balance of the numerical model may be computed, each of the terms must be converted to finite difference form in a manner consistent with that of the model equation of motion. How this is done is central to our analysis and is demonstrated in the remainder of this section. Some readers may wish to pass over the finite difference formula development, however, and for those we summarize its outcome in the next paragraph and defer them to the last two paragraphs of the section.

In the conversion to finite differences, terms 5, 6, 7 and 8 of Eq. (3.2) have straight forward representations based on second-order centered differences. However, the second term on the right of (3.1) is specially formulated by BB so that it conserves potential vorticity and potential enstrophy. The exact differential form of this term conserves these properties, but it is only as the grid point spacing tends to zero that a straight forward conversion to finite differences is conservative. As a result of the BB model's special conservative characteristics, when a finite difference vorticity equation is first developed from the equation of motion, as (3.2) is obtained from (3.1), the terms corresponding to 2, 3 and 4 include horizontal gradients of layer thickness and do not directly represent the traditional concepts of relative and planetary vorticity advection and stretching. The dependency on layer thickness variation may be split away, however, leaving terms which are easily related to 2, 3 and 4 and three additional terms, each of which vanishes in the one-layer, rigid-lid case. The model vorticity balance for the multilayer case contains, therefore, a three-part term which has no analog in (3.2) and which is directly related to the model's conservative properties. The relative importance of this term should decrease as grid point spacing is decreased, since those terms corresponding to relative and planetary vorticity advection and stretching will better approximate 2, 3 and 4 of the exact differential equation (3.2). All other finite difference terms constituting the model vorticity balance have direct analogs in (3.2) and will be related back to them.

In developing the finite difference form of the vorticity balance we first consider that of (3.1), as incorporated in the BB model, split here into the u- and v-components.

$$\left(\frac{\partial u}{\partial t}\right)_s = -\delta_x\left[\frac{1}{2}(\overline{u^2}^x + \overline{v^2}^y)\right] + \overline{v\delta_s p}^{xy}\,\overline{\left[\frac{\zeta_s+f}{\delta_s p}\right]}^{y} - \overline{(\delta_s p)^{-1}\overline{(\dot{s}\delta_s p)}^{x}\delta_s u}^{s} - \bar{\alpha}^x\delta_x\bar{p}^s - \delta_x\bar{\phi}^s$$
$$+ g(\delta_s p)^{-1}\delta_s\tau_x + A\overline{(\delta_s p)}^{x}[\delta_x(\overline{\delta_s p}^{xx}\delta_x u) + \delta_y(\overline{\delta_s p}^{xy}\delta_y u)] \quad (3.3)$$

$$\left(\frac{\partial v}{\partial t}\right)_s = -\delta_y\left[\frac{1}{2}(\overline{u^2}^x + \overline{v^2}^y)\right] - \overline{u\delta_s p}^{xy}\,\overline{\left[\frac{\zeta_s+f}{\delta_s p}\right]}^{x} - \overline{(\delta_s p)^{-1}\overline{(\dot{s}\delta_s p)}^{y}\delta_s v}^{s} - \bar{\alpha}^y\delta_y\bar{p}^s - \delta_y\phi^{-s}$$
$$+ g(\delta_s p)^{-1}\delta_s\tau_y + A\overline{(\delta_s p)^{-1}}^{y}[\delta_x(\overline{\delta_s p}^{xy}\delta_y v) + \delta_y(\overline{\delta_s}^{yy}\delta_x v)]. \quad (3.4)$$

The δ_Δ ( ) operator is the difference between ( ) at neighboring grid points divided by the Δ-direction grid distance. In the case of δ_s, the grid distance is unity. Similarly, $\overline{(\ )}$ is an average of ( ) over consecutive grid points. Here, ζ_s is defined as $\delta_x v - \delta_y u$ along a surface of constant s. From here on, we denote it merely as ζ.

To obtain the finite difference vorticity equation, we subtract $\delta/\delta y$ of (3.3) from $\delta/\delta x$ of (3.4):

$$\left(\frac{\partial \zeta}{\partial t}\right)_s = -\overline{u\delta_s p}^{xy\,x}\,\delta_x\left(\frac{\zeta}{\overline{\delta_s p}^{xy}}\right) - \overline{v\delta_s p}^{xy\,y}\,\delta_y\left(\frac{\zeta}{\overline{\delta_s p}^{xy}}\right) - \overline{u\delta_s p}^{xy\,x}\,\delta_x\left(\frac{f}{\overline{\delta_s p}^{xy}}\right) - \overline{v\delta_s p}^{xy\,y}\,\delta_y\left(\frac{f}{\overline{\delta_s p}^{xy}}\right)$$
(A) (B)
$$- \frac{\zeta+f}{\overline{\delta_s p}^{xy}}\overline{\delta_x(u\delta_s p)^{x} + \delta_y(v\delta_s p)^{y}}^{xy} - \overline{\delta_x[(\delta_s p)^{-1}\overline{(\dot{s}\delta_s p)}^{y}\delta_s v]}^{s} + \overline{\delta_y[(\delta_s p)^{-1}\overline{(\dot{s}\delta_s p)}^{y}\delta_s u]}^{s}$$
(C) (D)

$$- \delta_x\bar{\alpha}^{y}\overline{\delta_y p}^{sx} + \delta_y\bar{\alpha}^{x}\overline{\delta_x p}^{sy} + g(\delta_x\{(\overline{\delta_s p}^{y})^{-1}\delta_s\tau_y\} - \delta_y\{(\overline{\delta_s p}^{x})^{-1}\delta_s\tau_x\})$$

(E) (F)

$$+ A(\delta_x[\overline{(\delta_s p)^{-1}}^{y}\{\delta_x(\overline{\delta_s p}^{xy}\delta_x v) + \delta_y(\overline{\delta_s p}^{yy}\delta_y v)\}] - \delta_y[\overline{(\delta_s p)^{-1}}^{x}\{\delta_x(\overline{\delta_s p}^{xx}\delta_x u) + \delta_y(\overline{\delta_s p}^{xy}\delta_y u\}]) \quad (3.5)$$

(G)

where the signs are included in the lettered terms.

In the one-layer rigid lid case, terms (A), (B) and (C) of (3.5) reduce to simple finite difference analogs of relative vorticity advection, planetary vorticity advection and stretching, since the layer thickness $\delta_s p$, has no gradient and the references to layer pressure thickness, therefore, cancel. However, in the multilayer case, layer thickness is allowed to vary, and because the references to $\delta_s p$ in the numerator and denominator of those terms are averaged differently, they do not cancel. As mentioned above, this complication is introduced by the requirement that these nonlinear terms conserve potential vorticity and potential enstrophy. It is, therefore, desirable to break up these terms further into ones similar to the advection and stretching terms and others associated with the model's conservation properties. When we do so, term (A) becomes

$$-\overline{u\overline{\delta_s p}^{xy}}^{x}\frac{1}{\overline{\delta_s p}^{xy}}\delta_x\zeta - \overline{v\overline{\delta_s p}^{xy}}^{y}\frac{1}{\overline{\delta_s p}^{xy}}\delta_y\zeta$$

RVA

$$-\overline{u\delta_s p}^{xy\,x}\,\bar{\zeta}^{x}\,\delta_x\left(\frac{1}{\overline{\delta_s p}^{xy}}\right) - \overline{v\delta_s p}^{xy\,y}\,\bar{\zeta}^{y}\,\delta_y\left(\frac{1}{\overline{\delta_s p}^{xy}}\right),$$

EX1

where the first two components (RVA) are those which approximate the relative vorticity advection. Similarly (B) becomes

$$-\overline{u\overline{\delta_s p}^{xy}}^{x}\frac{1}{\overline{\delta_s p}^{xy}}\delta_x f - \overline{v\overline{\delta_s p}^{xy}}^{y}\frac{1}{\overline{\delta_s p}^{xy}}\delta_y f$$

BETA

$$-\overline{u\delta_s p}^{xy\,x}\,\bar{f}^{x}\,\delta_x\left(\frac{1}{\overline{\delta_s p}^{xy}}\right) - \overline{v\delta_s p}^{xy\,y}\,\bar{f}^{y}\,\delta_y\left(\frac{1}{\overline{\delta_s p}^{xy}}\right),$$

EX2

where the first two components (BETA) again approximate the planetary vorticity advection. In our case, the first half of BETA is zero, since there is no x-direction variation of the Coriolis parameter, f. Finally, term (C) becomes

$$-\frac{\zeta+f}{\overline{\delta_s p}^{xy}}\overline{(\delta_s p\delta_x u + \delta_s p\delta_y v)}^{xy}$$

STRCH

$$-\frac{\zeta+f}{\overline{\delta_s p}^{xy}}\overline{(u\overline{\delta_{xs}p}^{x} + v\overline{\delta_{ys}p})}^{xy}$$

EX3

where the term STRCH approximates the traditional stretching term.

RVA, BETA, and STRCH may now be easily related to terms 2, 3 and 4 of (3.2). In them remain references to layer thickness which do not cancel, but in comparing calculations with and without those references while examining the vorticity balances in several of our multi-layer experiments, we have found very minor differences. All horizontal gradients of layer thickness have been moved to EX1, EX2 and EX3. Our calculations have also shown that (D) and (E) of (3.5), representing the tilting/twisting term 5 and the solenoidal term 6 of (3.2), are zero or negligible for the experiments discussed here, apparently because there is very little if any exchange of fluid among the layers and, thus $\dot{s}$, $\nabla\alpha \sim 0$. Terms (F) and (G), representing the wind stress curl term 7 and viscous stress curl term 8 of (3.2), are subsequently referred to as WIND and VISC. The sum of EX1, EX2 and EX3 is referred to as CNSRV. As pointed out earlier, this term has no analog in the differential vorticity equation (3.2) and its value should tend to zero as grid spacing becomes finer. It is associated with the conservative properties of the numerical model, and we will show that it plays an important role in maintaining the model retroflection in multilayer experiments with 40 km resolution, but that its importance does indeed diminish when grid spacing is decreased to 20 km.

Assuming now that the terms of the vorticity equation are averaged over a long period during which statistical equilibrium exists, the local tendency is approximately zero, and the local vorticity balance may be stated as

$$\text{RVA} + \text{BETA} + \text{STRCH} + \text{CNSRV} + \text{WIND} + \text{VISC} = 0,$$

where, once again, RVA represents relative vorticity advection; BETA, planetary vorticity advection; STRCH, the vertical stretching; CNSRV, conservation of potential vorticity and potential enstrophy; WIND, wind stress curl; and VISC, the viscous stress curl.

4. The vorticity balance in a one-layer model

It is instructive to begin our discussion of the model vorticity balance with a very simple experiment to which linear theory can be directly compared. Such is LIN1, a linear, weakly viscous, one-layer experiment. Since the one-layer, rigid lid model has no divergent flow and no layer thickness variation, STRCH and CNSRV are equal to zero. And removing the advective terms from the model equation of motion eliminates RVA, so that the vorticity balance is among BETA, WIND and VISC. Spun up from rest, the circulation becomes steady after a few hundred days. The steady solution (LIN1) (Fig. 2a) has essentially the same characteristics as the linear analytical solution of de Ruijter (1982). Here the maximum wind curl is slightly north of the tip of Africa, so that a small portion of the subtropical gyre closes near the tip. Along the no-slip coast of Africa in the Munk layer, lateral friction (Fig. 2c) balances the β-induced input of relative vorticity (Fig. 2b). The magnitude of the latter is determined by the southward velocity, which is governed by the combination of integrated wind curl and layer depth, as well as friction. WIND is very small relative to BETA and VISC in the western boundary current, but the latter two are much smaller east of the boundary current, explaining the lack of exact balance between them there (Fig. 2b, c and Fig. 3b, c). In the low viscosity case (LIN1), the boundary layer is relatively thin and friction becomes very small after separation, and therefore, so does the planetary vorticity advection. In this linear solution, which possesses very little eastward Sverdrup flow north of Africa's tip, almost all the flow responds to this condition by turning westward into the Atlantic.

If we increase viscosity by an order of magnitude to 3300 $m^2 s^{-1}$ (LIN2) (Fig. 3), friction becomes important in the area south of Africa. Some fluid can continue southward a distance since BETA (Fig. 3b) can be balanced by VISC (Fig. 3c). In other terms, the frictional boundary layer is broadened enough so that more streamlines of the current reaching Africa's tip are able to connect with returning Sverdrup lines to the south and, thus, establish a partial retroflection. Therefore, nonlinear effects are not required in order to obtain retroflection.

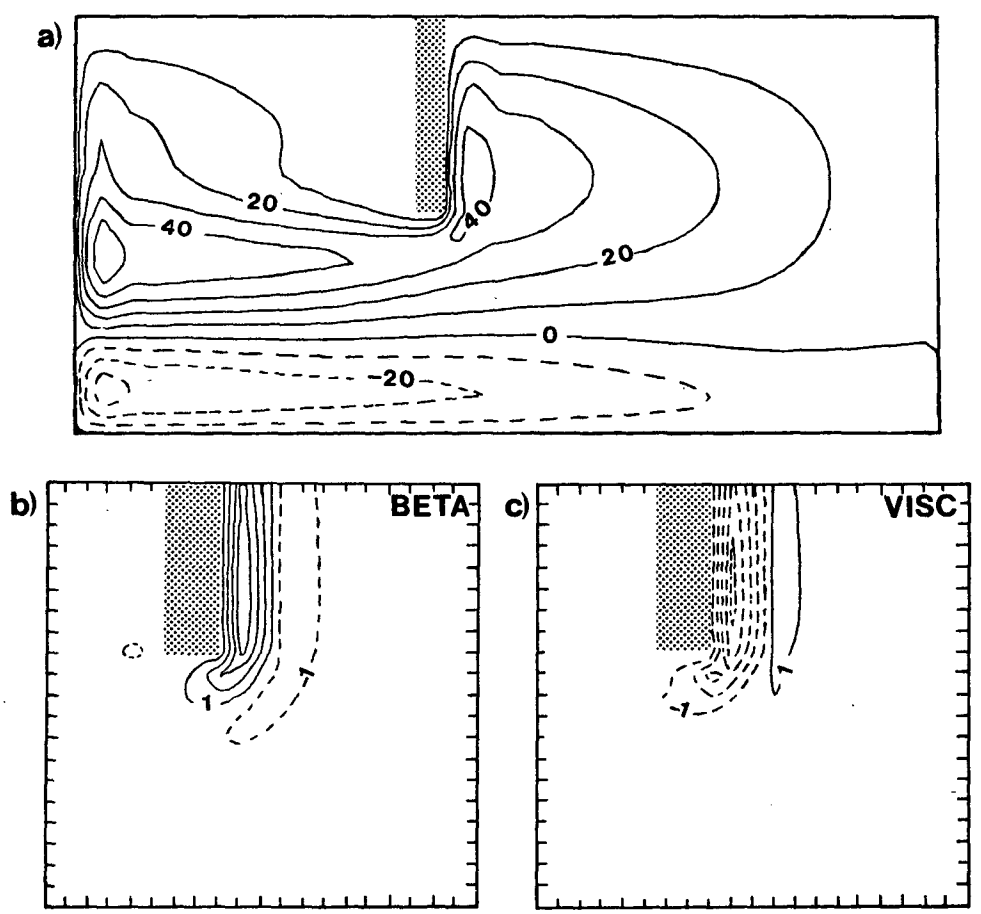

FIG. 2. Experiment LIN1. (a) The mean mass transport streamfunction. The contour interval is 10 Sv. (b) The distribution of planetary vorticity advection BETA around the southern tip of Africa for the steady solution. The contour interval is 2×10^{-12} s^{-2}. (c) As in (b), except viscous stress curl VISC.

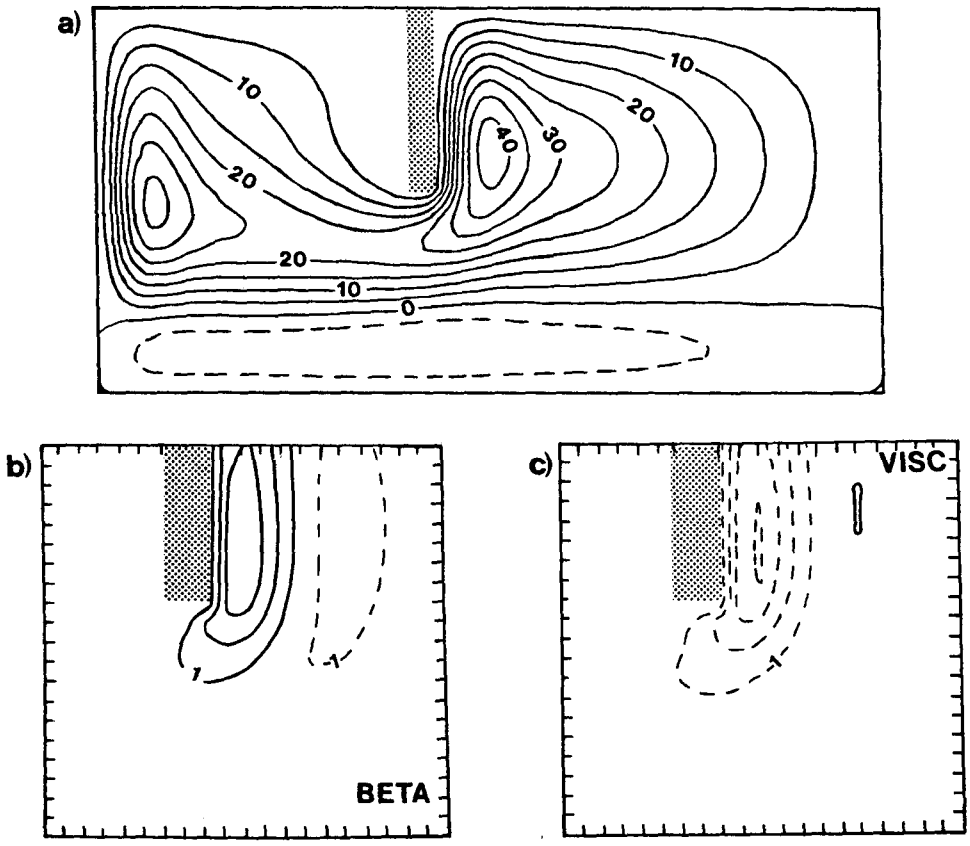

FIG. 3. Experiment LIN2. As in Fig.2, except the contour interval is 5 Sv in (a).

Important to note, this value of eddy viscosity (3300 $m^2 s^{-1}$) is an order of magnitude larger than that normally used in eddy-resolving models to parameterize subgrid-scale turbulence, but it is several times smaller than that required in coarse-resolution models. Thus, if Agulhas retroflection is obtained in coarse-resolution calculations ($\Delta x > 100$ km), it may be dominated by the balancing of planetary vorticity advection with viscous stress curl.

Introducing the inertial terms adds relative vorticity advection [(RVA) in (3.3)] to the balance. Experiments NLIN2 (Fig. 4) and NLIN1 (Fig. 5) correspond respectively to the nonlinear runs of LIN2 and LIN1. First, considering the high viscosity case (NLIN2), most of the retroflection is moved south and west of the tip of Africa, but the general characteristics of the flow pattern are unchanged (Fig. 4a). Inclusion of the inertial terms results in an increase in the seaward diffusion of the negative relative vorticity generated at the coast. This is because the total velocity is a bit stronger and the boundary layer, now inertial–frictional, is thinner. The planetary vorticity advection (Fig. 4b) does not increase, however, since the orientation of the retroflection gains a SW–NE tilt. The increase in VISC (Fig. 4d) is balanced by the new term RVA (Fig. 4c). In contrast to the more weakly viscous experiments to follow, RVA is in the mean flow only, since the flow pattern becomes steady after a year. The marked change in VISC after separation is also balanced by RVA and derives from the fact that the Agulhas now separates from Africa at the southeast tip of the rectangle. The decrease in velocity from the current core to the coast is now resolved by the grid. This feature complements the β-effect by adding positive vorticity and encouraging retroflection just south of the tip. The major conceptual difference from LIN2 is that the fluid may now flow southward from the tip of Africa due to its own inertia. Friction, however, is still dominant.

In the corresponding low viscosity case (NLIN1) the boundary layer is relatively thin and friction is much less important than inertia after separation. This leads to substantial modification of the flow pattern and the distribution of terms in the model Agulhas' vorticity balance (Fig. 5). The recirculation gyre immediately east of Africa is shifted southward due to inertia, and the coastal Agulhas is narrower, having slightly greater maximum velocity. A primary change in VISC (Fig. 5d) along the coast is that it is important only within the current core and westward to the coast. The region where BETA (Fig. 5b) is relatively large also has less east–west extent, but more than VISC, so that now RVA (Fig. 5c) balances BETA on the offshore side of

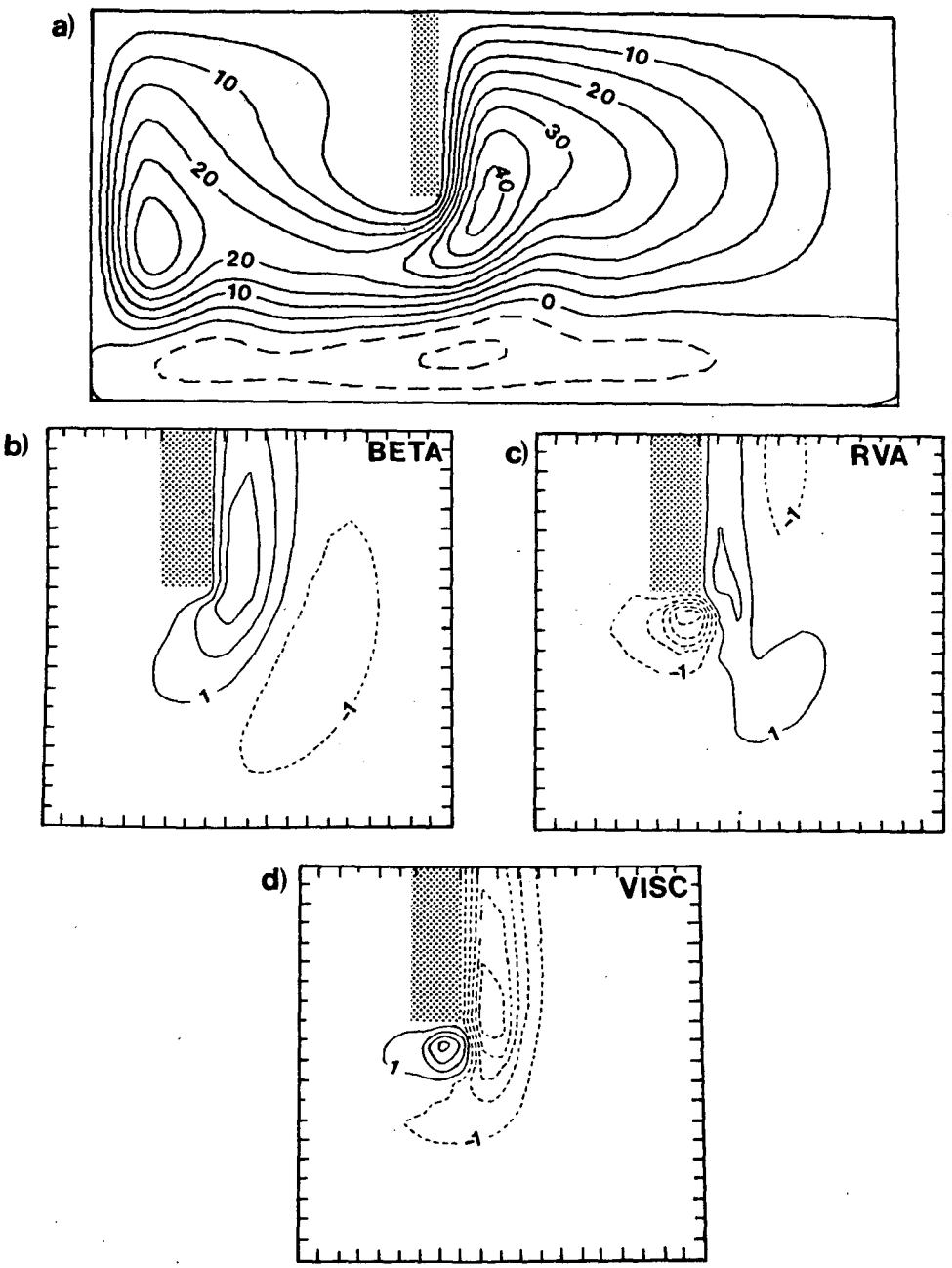

FIG. 4. Experiment NLIN2. As in Fig. 3 for (a) and (b). (c) Distribution of relative vorticity advection. (d) As in Fig. 3c.

the current core. This is in contrast to the highly frictional case (NLIN2) in which VISC is so large throughout the coastal Agulhas that BETA and RVA complement each other there to maintain a balance (Fig. 4b, c, d). Here in NLIN1, VISC is large only next to the coast and shares the role of balancing BETA with RVA. In this model, then, viscous effects can determine the magnitude and sign of the mean value of relative vorticity advection. The magnitude of VISC is strongest in NLIN1 just beyond Africa's tip where the horizontal shear is still very great. Only here is a positive maximum in RVA required to complement BETA in balancing VISC.

In each of LIN2, NLIN1 and NLIN2, there is a substantial retroflection. The similarity among all three is the establishment of a boundary layer south of Africa in which the β-effect is balanced by the turning eastward of a major portion of the current. In LIN2 the boundary layer is purely frictional, in NLIN2 it is frictional–inertial, dominated by friction, and in NLIN1 it is pri-

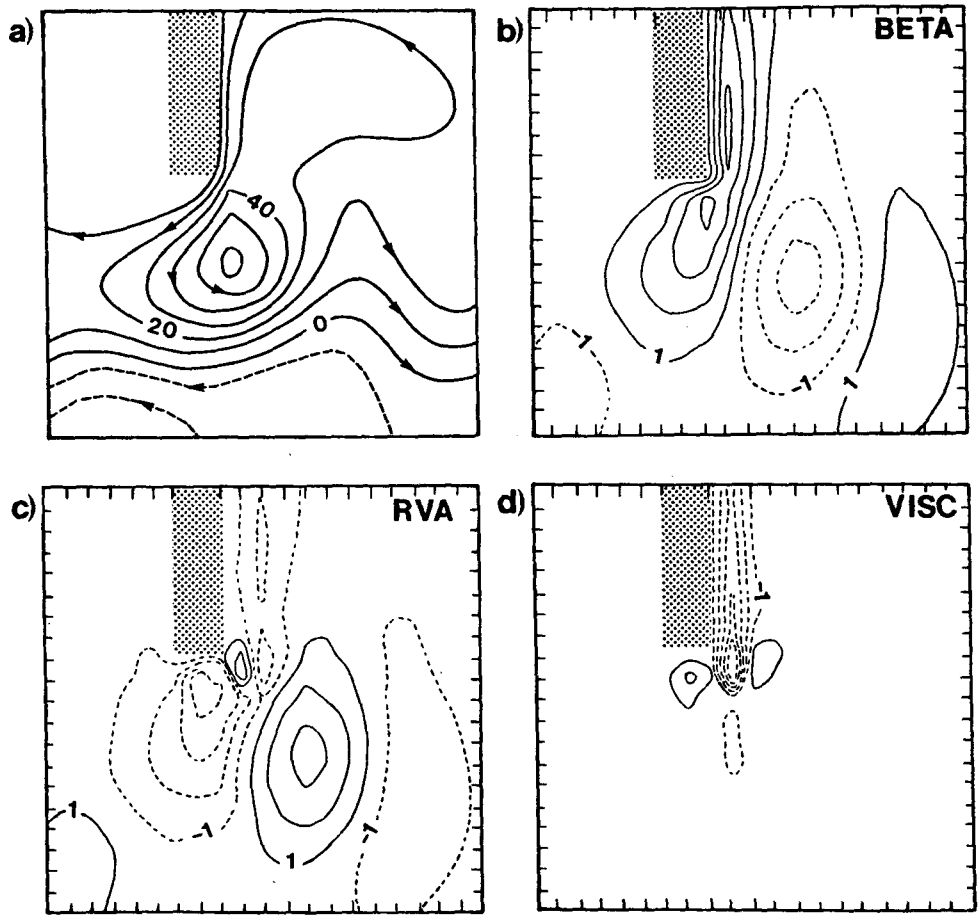

FIG. 5. Experiment NLIN1. (a) The upper layer mean mass transport streamfunction around the tip of Africa for the final 1825 days of the 3650 day experiment. The contour interval is 10 Sv. As in Fig. 4 for (b), (c) and (d), averaged for the same period as in (a).

marily inertial. While the physical mechanism of retroflection is not the one proposed by de Ruijter (1982)—the inertial overshooting distance—his concept of the retroflection being accomplished within a free inertial boundary layer is apparently applicable. In the experiments remaining to be discussed, the retroflection is accomplished in this type of boundary layer. The vorticity balance of NLIN1 has a character similar to that of the least nonlinear of the multilayer cases and will be discussed further along with them.

5. The vorticity balance in the multilayer model

a. Variation of inertia and baroclinicity

As described in BD, the strength of the retroflection in the multilayer model depends on the nonlinearity/baroclinicity of the flow. For these experiments, only the vorticity balance of the top layer, the one in which most of the wind-driven circulation resides, is examined. The similarity in retroflection regimes between NLIN1 and that in the top layer of the least nonlinear/baroclinic multilayer experiment (E1) is suggested by the similarity in the vorticity balances, to be demonstrated shortly. STRCH and CNSRV begin to play important roles, however, as the upper ocean Rossby number increases, and, proceeding to E2 and E3, where the mean top layer thickness decreases from 1000 db first to 600 db and then to 300 db, the flow patterns and retroflection vorticity balance are greatly transformed.

These four experiments have high temporal variability, as opposed to LIN1, LIN2 and NLIN2, which reach steady states after relatively short spinup times. To identify the contribution from the transients, RVA and STRCH have been separated into components associated with the mean and transient eddy flow fields. The two components of RVA have comparable magnitudes but generally opposite sign in the experiments with highly transient retroflection flow patterns, i.e., ones in which rings are continually being formed. In those experiments, the total RVA fields have much smaller maxima and minima and quite different struc-

tures than either of their components. This is especially the case in NLIN1, E1 and the final experiment E11. In the remaining experiments, which have strong, relatively steady retroflections, the contribution from the mean flow is the dominant one, and that from the eddies partially cancels it. In all experiments, the dominant contribution to STRCH is from the mean flow component. Other than through this general characterization, the individual mean and transient components of RVA and STRCH do not possess information helpful in understanding the model vorticity balance and are, therefore, not addressed further here.

1) VORTICITY BALANCE ALONG THE COAST

The model Agulhas' vorticity balance along the coast is illustrated in Fig. 6 for NLIN1, E1, E2 and E3, in the same fashion as done by Bryan (1963) and Holland and Lin (1975). CNSRV is not displayed because of its very small values north of Africa's tip in all experiments. It is seen that close to the coast (at grid point 1, 40 km offshore), viscous effects are important in each case. As noted by DB, negative relative vorticity is generated by the no-slip boundary condition and then transported eastward by diffusion. The value of

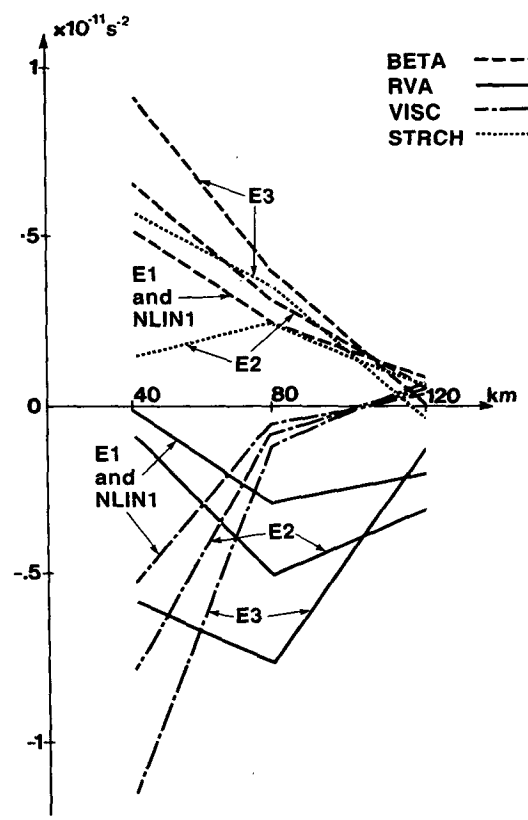

FIG. 6. Values of BETA, RVA, VISC and STRCH averaged along the coast of Africa for NLIN1, E1, E2 and E3 at the first three grid points from the boundary.

STRCH in E1 is negligible north of Africa's tip, and the NLIN1 and E1 balances along the coast are almost identical, so separate curves for the two experiments are not plotted. In both, VISC and BETA approximately balance next to the coast, giving way to a balance between BETA, RVA, and a much smaller VISC away from the coast.

BETA, VISC and STRCH increase from E1 to E3. In E2 the principal balance is between BETA and VISC next to the coast. In E3, BETA and VISC are primary terms in the balance, but the secondary terms RVA and STRCH have equal and opposite magnitude, about half that of the primary ones. Moving further away from the no-slip boundary VISC rapidly decreases in magnitude, as in E1 and NLIN1, and RVA increases. STRCH slightly increases in E2 and decreases in E3. In both cases BETA decreases. STRCH and BETA are still generating positive relative vorticity, however, as they are next to the boundary, and are now balanced by RVA. At 120 km from the coast, which is at the outer edge of the boundary current, BETA, RVA, STRCH and VISC have become small, and are of the same order of importance as WIND (not pictured).

It may be stated, then, that in each of these experiments, the principal vorticity balance in the current core, the part closest to the coast, is between planetary vorticity advection and viscous stress curl, such that the positive relative vorticity generated by the former mixes with the negative vorticity generated at the boundary, rather than appearing as increased anticyclonic shear or curvature, or by thickening of the layer. Just east of the core, viscous effects are much less important and positive generation by planetary vorticity advection and stretching is balanced by negative relative vorticity advection. At the outer edge of the coastal Agulhas, these terms are quite small and of the same order of importance as the wind stress curl.

2) RETROFLECTION VORTICITY BALANCE

As in NLIN1 (Fig. 5a), the Agulhas in E1 separates at the sharp change in coastal orientation, the southeast tip of Africa (Fig. 7a). The mean flow patterns and the distribution of BETA, RVA and VISC in the retroflection region are rather similar between the two experiments (compare Fig. 5 with Fig. 7a, b, c, d). It is noted also, however, that the stretching term (Fig. 7e), unimportant before separation, is the same order of magnitude as BETA in the retroflection south of Africa. On examining the linear $(-f\nabla\cdot\mathbf{V})$ and nonlinear $(-\zeta\nabla\cdot\mathbf{V})$ components of STRCH, we have found the nonlinear to be much smaller in magnitude than the linear. The STRCH term, therefore, can be assumed to be proportional to the divergence of the mean flow. This is in agreement with our finding that the mean flow component of STRCH dominates that from the transient eddies. There is, thus, mean divergence associated with the west side of the separated current,

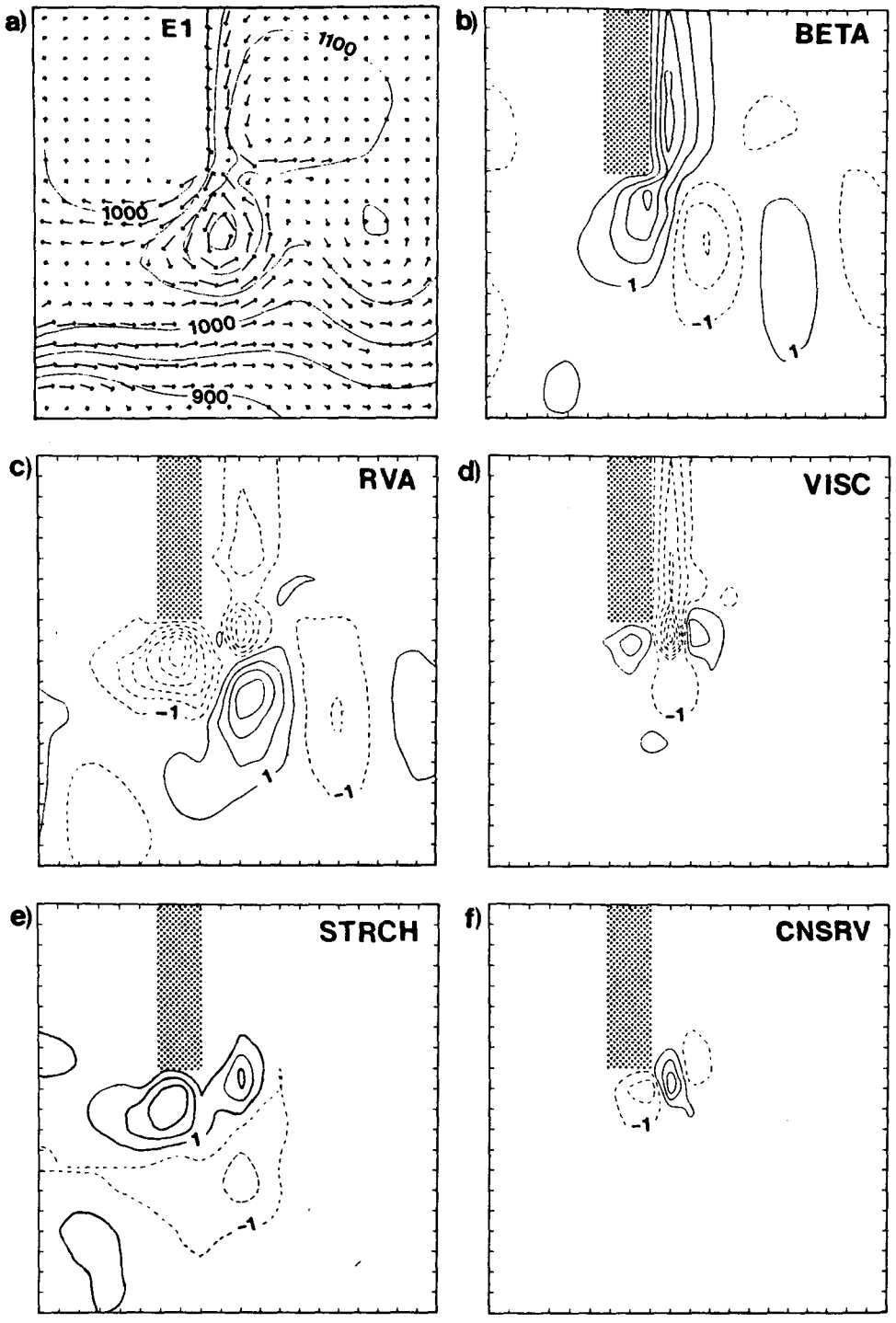

FIG. 7. Experiment E1. (a) Mean flow pattern and thickness for Layer 1 for the last half of the 3650 day experiment. A full length arrow and each additional barb represent a velocity of 0.25 m s^{-1}. Arrows are plotted for each grid box. The contour interval for layer thickness is 50 db. As in Fig.5 for (b), (c) and (d). (e) The time mean distribution of the stretching term STRCH. (f) The time mean distribution of the sum of the terms resulting from conservation of potential vorticity and potential enstrophy CNSRV.

including the area where the leakage is fanning out as it branches away from the retroflection toward the Atlantic, and on the northeast side of the retroflection eddy. The tendency is to add positive relative vorticity and keep the fluid circulating anticyclonically. Conversely, on the south and southeast side of the retro-

flection, mean convergence generates negative relative vorticity, allowing some fluid to escape the retroflection eddy into the Agulhas Return Current. Comparing Figs. 7b and 7e, we note that STRCH mostly complements BETA, and one result is that the latitudinal scale of the retroflection is smaller than in the one layer model (e.g., compare Figs. 5a, b, c and 7a, b, c, which display the same portion of the basin).

This important difference between the one layer model, as well as quasi-geostrophic (QG) models, and multilayer primitive equation (PE) models is a consequence of the nonlinearity of the mass continuity equation (the thermodynamic equation in depth coordinate models) in the presence of stratification. Layer thickness perturbations in barotropic and QG models are assumed to be zero or very small with respect to the mean thickness of the layer. In those models, it is appropriate, therefore, to view the continuity equation as linear and the contribution from the stretching term as relatively unimportant or zero. In stratified PE models, excursions of isopycnals from their mean depth may be as large, or larger than, their mean depth. With the allowance of these displacements, an important new consideration enters the vorticity balance. This nonlinearity is most easily understood in the BB model by breaking up the right side of the continuity equation as follows (assuming $\dot{s} = 0$):

$$\frac{\partial}{\partial t}\left(\frac{\partial p}{\partial s}\right) = -\frac{\partial p}{\partial s}\nabla\cdot\mathbf{V} - \mathbf{V}\cdot\nabla\frac{\partial p}{\partial s}.$$

If the system is in statistical equilibrium,

$$\frac{\partial}{\partial t}\left(\frac{\partial p}{\partial s}\right) \sim 0,$$

and the temporal mean value of

$$-\left(\frac{\partial p}{\partial s}\right)^{-1}\mathbf{V}\cdot\nabla\frac{\partial p}{\partial s}$$

may be substituted for that of $\nabla\cdot\mathbf{V}$ into the stretching term 4 of (3.2). This nonlinear term is thus proportional to the ratio of layer thickness gradients to total layer thickness.

In the E1 retroflection vorticity balance, the importance of STRCH results from the fact that relatively large gradients in layer thickness are generated, so that the mean contribution from the above thickness advection term cannot be ignored. In the retroflection region, instantaneous deviations of layer-1 thickness from its horizontal mean, which are somewhat larger than those shown here for the temporal mean mass-flow field (Fig. 7a), are fairly small with respect to the total (about 10%). However, comparison of Figs. 5 and 7 suggests that they are not negligible.

The contribution from the special terms required for potential vorticity and potential enstrophy conservation, CNSRV (Fig. 7f), whose importance is also related to the existence of layer thickness gradients, is a relatively small part of the vorticity balance and is only significant very close to separation. Just east of the current core, it generates positive vorticity and on the west side negative. Since the significant values occupy such a small region, however, we conclude that CNSRV is relatively unimportant to retroflection strength in E1.

With the exception of the STRCH term, the retroflection vorticity balance for E2 (not illustrated) is much the same as in E1. The mean top layer thickness is 40% less, so that the layer-1 velocities are ~40% greater, and all terms have maximum values at least 30%–40% larger than in E1. But STRCH becomes even more aligned with BETA and its maximum values are greater than those in BETA. Each component of the above substitution from the continuity equation favors larger values of STRCH: the inverse of layer thickness, thickness gradients and velocity. The fluid in the separating current, whose linear tendency is to turn westward into the Atlantic (Fig. 2) is encouraged by both STRCH and BETA to remain within the retroflection, and, when it reaches the east side of the retroflection eddy, headed north, both effects support leaving the retroflection in an eastward direction. The net effect is to strengthen the retroflection.

Exchange of fluid between the model Indian and Atlantic oceans is all but shut off in E3, (Fig. 8a), which has horizontal mean top layer thickness half that of E2, 300 db. This dramatic difference from the previous experiments is accompanied by equally large changes in the retroflection vorticity balance. The great strength of the retroflection is easily understood in that not only is the southward velocity at separation almost double that in E2, yielding a doubling of BETA, but each component of STRCH (Fig. 8e) (as redefined above through substitution from the continuity equation) is substantially larger. Only a very small part of the current turns westward into the Atlantic. While the primary balance is between BETA and VISC before separation, as shown in Fig. 6, the major components of the balance in the retroflection region are STRCH and RVA, the maximum values of which are as much as three times that of BETA (Fig. 8b). The larger values of STRCH extend along the current southward from separation, adding positive relative vorticity, to the point where the current has turned back toward the Indian Ocean.

In areas where motion is toward smaller values of layer thickness, STRCH contibutes positive vorticity, strengthening the retroflection, and the magnitude of the contribution increases as layer thickness decreases. In the overshooting current, therefore, motion out of the retroflection toward the west or south is, in the mean, accompanied by a gain in positive vorticity, turning the fluid back toward a retroflecting pattern.

The particularly large values of STRCH near the separation can be understood, more so than in E1 and E2, from the standpoint of the changing environment

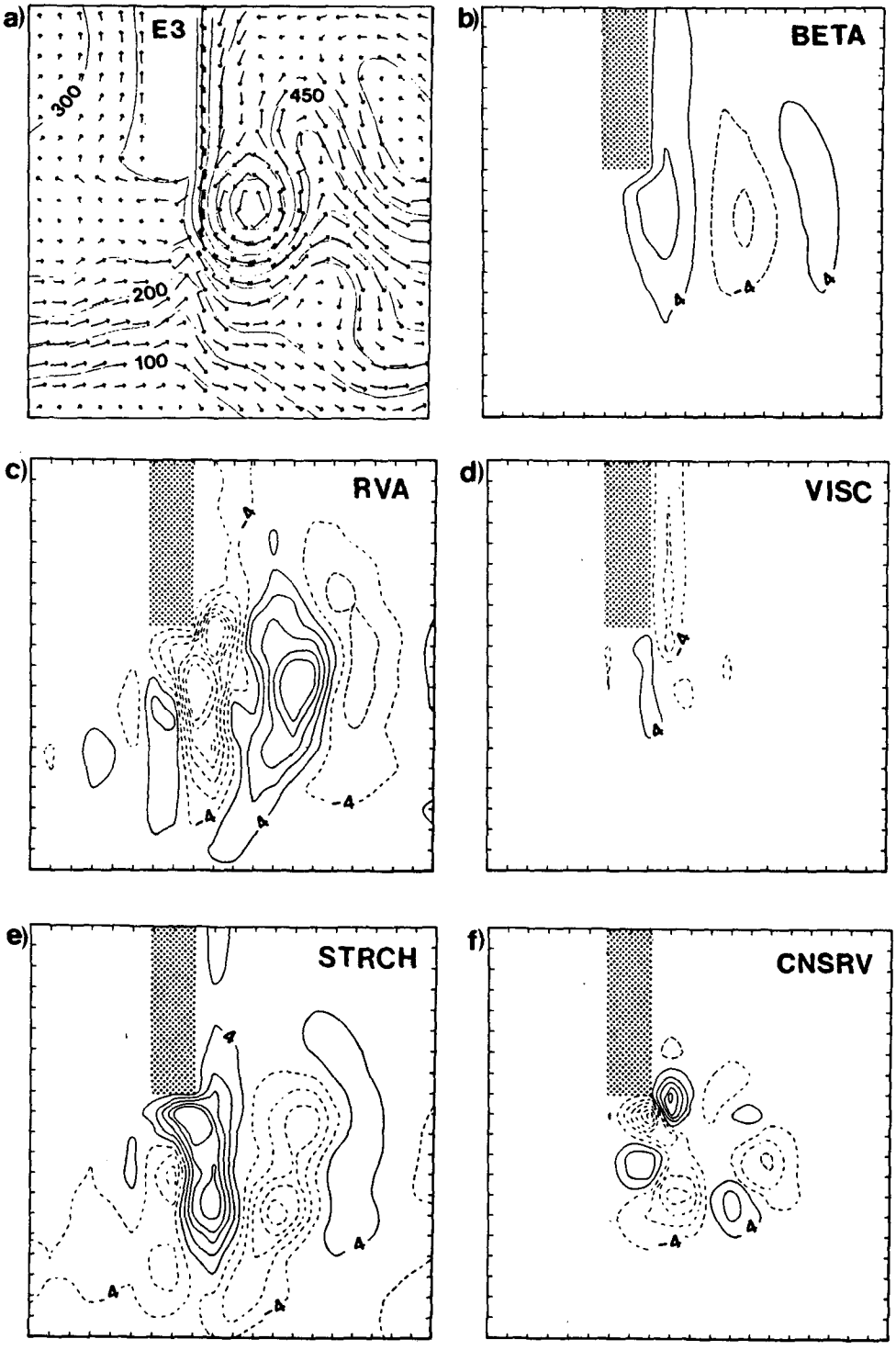

FIG. 8. As in Fig. 7, for Experiment E3, except the contour interval in (b), (c), (d), (e) and (f) is 8×10^{-12} s^{-1}.

which the fluid experiences there. First of all, it leaves the no-slip boundary, a large sink of momentum, for the open ocean. This leads to some immediate acceleration and thus divergence (positive STRCH). Secondly, the juxtaposition of a layer thickness of ~360 db on the western edge of the coastal Agulhas and ~275 db at the eastern edge of the subtropical South Atlantic leads to an increased isopycnal tilt at the west-

ern edge of the separated current. Through the thermal wind relation, this also leads to acceleration of the southward motion and layer-1 divergence. Because of the smaller contrast in juxtaposed layer thicknesses (and, thus, potential vorticities) this effect plays a much smaller role in E1 and E2.

In addition to the increased importance of the stretching term in E3, it is evident from Fig. 8f that the sum of terms resulting from conservation of potential vorticity and potential enstrophy plays an important role. The change from E1 is undoubtedly due to the much stronger gradients of layer one thickness in E3. Because of the alternating positive and negative values in CNSRV, proceeding around the retroflection, it is not as easy as with STRCH to conclude its overall effect on retroflection strength. However, an experiment otherwise similar to E3 has been run without reference to layer thickness in the finite difference form of the 2nd term on the right of (3.1)—that is, without the aforementioned conservative qualities. In this nonconservative experiment (not illustrated here), there is relatively steady leakage and regular formation of Agulhas rings which drift westward into the Atlantic, much as in E1 and E2. On the basis of this simple intercomparison, we conclude that conservation of potential vorticity in the separating current is essential to the strong retroflection generated in E3.

Boudra and de Ruijter show that E8, of which the only parametric difference from E3 is the addition of linear bottom drag, is marked by an even more intense retroflection. The retardation of bottom layer flow apparently enhances the vertical shear associated with the retroflection, so that mean top layer velocities in the eddy are stronger and the layer thickness gradient greater than in E3. The mean layer thickness now changes by 400 db from the center to the outer edge of the retroflection eddy. This results in approximately 10% increases in the maximum values of BETA, STRCH and RVA, but the horizontal structure of the retroflection vorticity balance is as in E3.

b. Horizontal resolution

As pointed out by BD, 40 km horizontal resolution cannot adequately describe the details of boundary layer flows. While an order of magnitude decrease in grid spacing would be necessary to do this, such is computationally prohibitive. They performed an experiment with grid spacing halved (E10), however, in order to test the sensitivity of the model retroflection to improved resolution of the boundary layer and release of baroclinic instability. This produced a number of minor changes in the retroflection mean flow pattern, which may be noted comparing Figs. 8a and 9a. There is even less leakage into the Atlantic in E10 and the retroflection eddy is not as closed on the north side. In turn, the cyclonic meander east of the eddy is higher in amplitude. Also, the eastward drift representing the northern edge of the ACC remains farther south than in E3 and E8. This characteristic is important in allowing four rings which form in E10 to drift westward into the Atlantic before being recaptured by the retroflecting current (see Chassignet and Boudra, 1988). Ring formation and drift into the Atlantic does not occur in E3 or E8. These refinements likely result from the increased eddy activity in E10, which is a consequence of enhanced release of instabilities.

An increased maximum velocity in the coastal Agulhas is indicated by the greater value of BETA (compare Figs. 8b and 9b), which is directly proportional to the mean southward velocity. The boundary current is better resolved, and as anticipated, its cross stream profile has changed. This results in a much greater increase in VISC (compare Figs. 8d and 9d) than in BETA, however, and the higher value of VISC along the coast is now balanced by both RVA (Fig. 9c) and STRCH (Fig. 9e). A fundamental change, then, from NLIN1 and the 40 km resolution multilayer experiments is the change in the vorticity balance in the core of the coastal Agulhas. In those experiments the balance is chiefly between planetary vorticity advection and viscous stress curl. As the coastal current structure changes with better resolution, the eastward diffusion of negative vorticity is balanced by positive generation due to approximately equal components of planetary and relative vorticity advection and stretching. If resolution were further improved, some additional evolution of the balance might be expected, but because of the computational expense, this must be left for future work.

As in previous experiments, the value of VISC decreases rapidly east of the current core, and positive generation by STRCH and BETA balance RVA. About 60 km north of Africa's tip, STRCH begins to increase rapidly, as in E3 (Fig. 8e), toward its maximum value in the current core just beyond separation at the tip. Again, this is most likely due to the changing physical environment as the fluid leaves behind the no-slip boundary, and in its place is the eastern subtropical South Atlantic water mass with smaller layer-1 thickness (larger negative potential vorticity) than that of the western edge of the Agulhas along the coast. Beyond the immediate separation region, BETA and STRCH complement each other with STRCH approximately twice the size of BETA. As in the previous cases, this discourages the fluid from leaving the retroflection in the westward direction associated with the linear solution (Fig. 2) and, after turning eastward and then northward, STRCH favors continued eastward motion.

An additional refinement brought about by improved horizontal resolution is a reduction in the role of the terms included to ensure potential vorticity and potential enstrophy conservation, CNSRV (Fig. 9f). Comparing with CNSRV in E3 (Fig. 8f), we see that while the maximum values just at separation are larger in E10 than E3, the horizontal scale over which

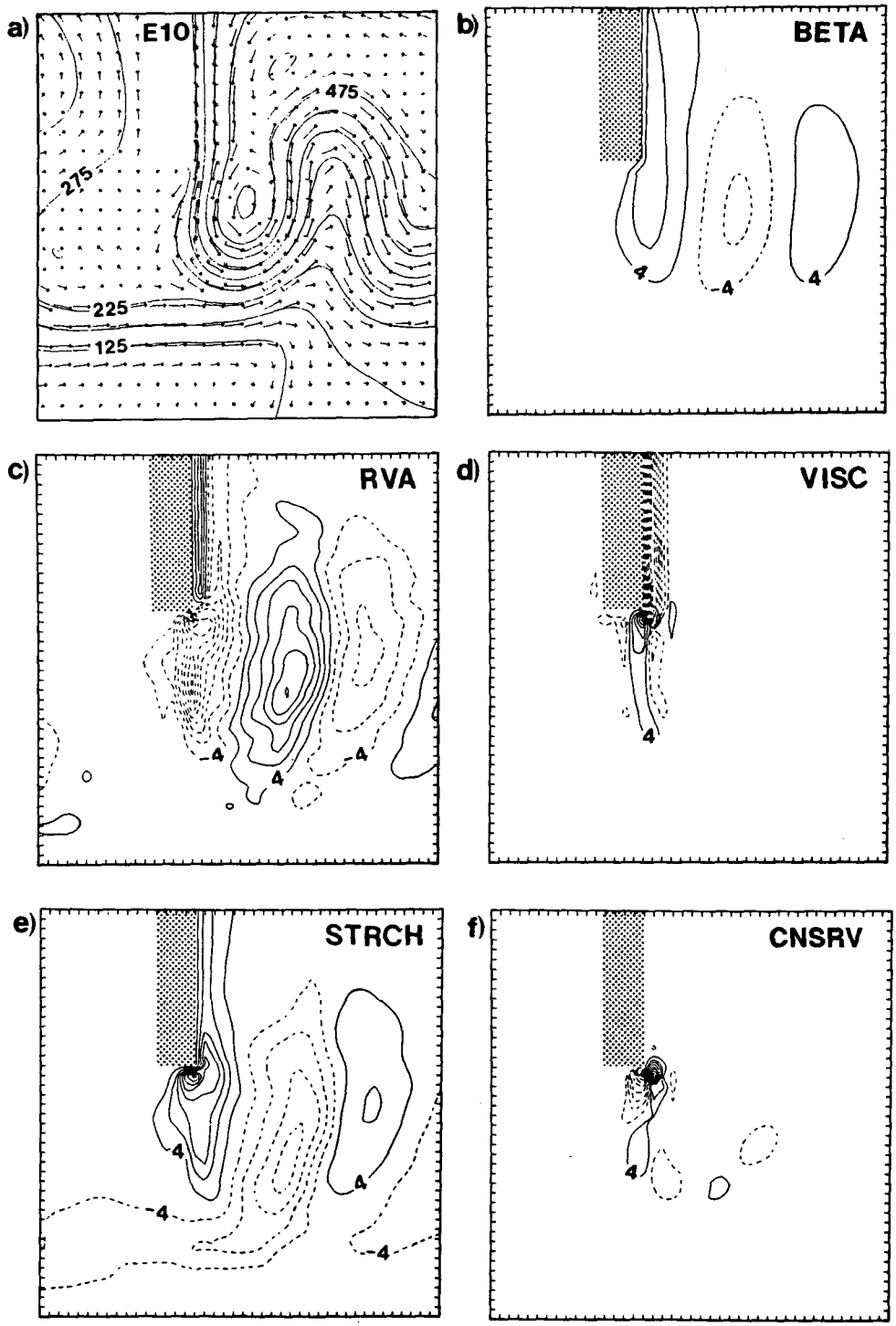

FIG. 9. As in Fig. 8, for Experiment E10, except that in (a) arrows are plotted only for every other grid box.

CNSRV is the same order of magnitude as the other terms is much smaller. A 20 km resolution experiment without the conservative characteristics has not been run, but given the reduced importance of CNSRV in the retroflection vorticity balance, it is expected that this would not greatly weaken the retroflection as it does with 40 km resolution. Comparison of E10 with E3 and E8 suggests that, as the numerical model resolution is improved, so that the model becomes more conservative without inclusion of special terms, the

Agulhas retroflection remains a prominent feature of the solution. With further reduction of the grid spacing, the importance of CNSRV would continue to decrease. At the same time, it is suggested that the strength of the retroflection, shown in the previous section to depend on conservation of potential enstrophy, would not diminish.

c. *Boundary condition along the African coast*

In the above discussion, the importance of the viscous stress curl VISC in the coastal current vorticity balance has been pointed out. Especially in the 40 km resolution experiments, the primary balance next to the coast is between BETA and VISC. With 20 km resolution VISC becomes much greater and positive generation by both RVA and STRCH add to that due to BETA in order to balance the loss through VISC. Boudra and de Ruijter conducted a 40 km resolution experiment (E9) with a free-slip boundary condition on Africa in order to gain more insight into the role of boundary layer friction in the retroflection strength. The boundary layer must still be considered more highly frictional than the interior since velocity shears are much greater, but the free-slip condition implies no momentum exchange between the fluid and the boundary. We thus characterize the free-slip and no-slip boundary conditions as weakly and strongly frictional, respectively.

A very different two-basin flow configuration was obtained in E9. In the corresponding no-slip case (E8), for which the retroflection mean flow pattern is quite similar to that in Fig. 8a for E3, only a small amount of fluid escapes into the Atlantic. In the free-slip experiment, most of the fluid hugs the coast and makes the turn into the Atlantic (Fig. 10a).

In the top layer vorticity balance for E9 (Fig. 10b–f), it is seen that VISC is negligible in comparison to RVA, BETA and STRCH except in the immediate vicinity of Africa's southern tip. The principal balance is among these three terms in the southward flowing boundary current. Contrary to the no-slip case, there is no cyclonic vorticity present along the coast.

In order to overshoot the tip (and afterward retroflect) the current must coexist with a region beyond its western edge which is largely motionless (a good example is shown in Fig. 9a for E10). In the no-slip case, the western boundary condition for the current along the coast is already a motionless one. Thus, provided inertia is strong enough to overcome the linear tendency to make the sharp turn (Fig. 2), the current shoots past the tip in a relatively natural fashion, as shown here for E3 (Fig. 8a) and E10 (Fig. 9a). In contrast, the condition at the western edge of the coastal current in the free-slip case (E9) results in the current having its maximum value there. In an overshooting configuration, it would have to adjust to a strongly sheared condition. Instead, the E9 circulation pattern south of Africa is a highly turbulent one in which rings form next to the southern coast quite often and, occasionally, a substantial portion of the current retroflects. But, in the mean, the major portion of the current stays close to the boundary along which the shape of its cross-stream velocity profile can remain intact, first turning westward and then northward around the southern tip of Africa. That these abrupt turns involve vigorous and highly variable flows is suggested by the relatively large values of RVA, STRCH, VISC and CNSRV surrounding the tip, emphasizing the physical strain imposed on the mass–flow structure and, thus, the strong controlling influence of the boundary condition.

6. South African coastal geometry

At the end of their paper, BD recognize that the shape and orientation of Africa in their experiments is one which maximizes the importance of the β-effect in the model retroflection. Here, we have determined that the stretching term, through which the adjustment of the separating Agulhas to its free ocean environment is expressed, is at least as important in the retroflection strength as the βv term. Inasmuch as β plays one of the important roles, however, configuring the coastal geometry such that the relative importance of this term is realistic seems warranted. After leaving the South African coast, the real Agulhas flows along the Agulhas Bank shelf break, which is oriented approximately from northeast to southwest, thereafter continuing past the tip of the Bank into the deep ocean (e.g., see Lutjeharms, 1980). In this configuration, the component of velocity advecting planetary vorticity is about 70% of the total, rather than 100%, as with the meridionally oriented coast of BD's model. The basin geometry shown in Fig. 11 has been chosen, therefore, as a next step toward model realism.

In this section, we wish to describe a high resolution experiment on this new geometry by discussing the 1) mass transport streamfunctions for layers 1 and 3 averaged over the last half of the 3650 day simulation (Fig. 12) and 2) the retroflection vorticity balance. It should be noted that approximately 10% of the subtropical Indian Ocean is converted to land in this new basin, so that the linear Sverdrup transport is smaller along the boundary northeast of Africa's tip. This in itself will result in some difference from the previous solutions even though the Sverdrup transport is the same as before at the tip of Africa (about 45 Sv). With this in mind, our comparison of E10 and E11 should be viewed mainly qualitatively.

a. *E11 mean flow pattern*

The top and bottom layer flow patterns (Figs. 12 and 13a) for this new 20 km resolution experiment (E11) bear many of the same characteristics as those

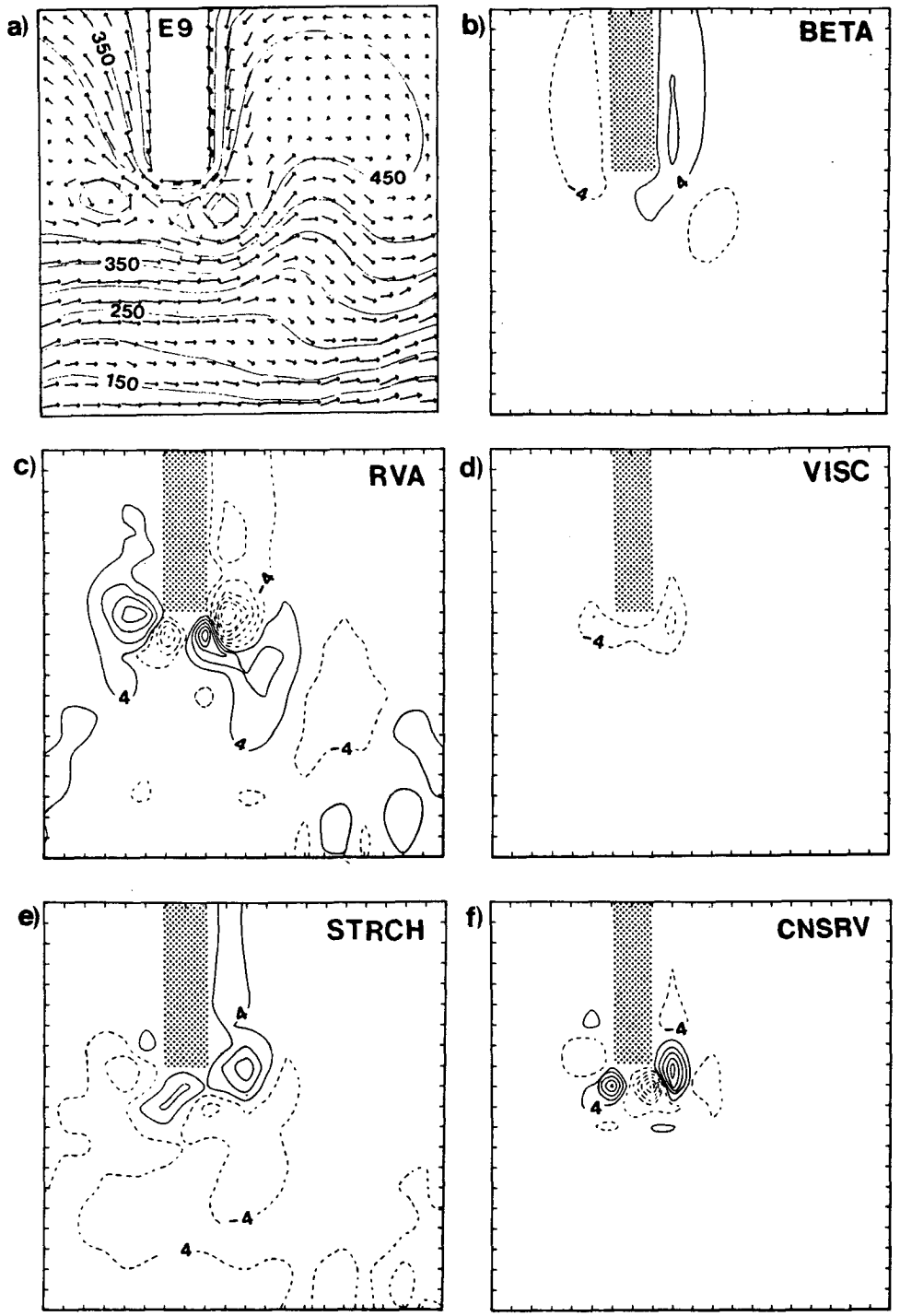

FIG. 10. As in Fig. 8 for Experiment E9.

of E10 (for comparison, see Fig. 13 in BD). There are some notable differences, however, especially in the Indian Ocean sector. The retroflection is still strong, but less intense. The mean Agulhas along the coast is somewhat broader, and its maximum velocity is less than in E10. With the tilted coast, fluid in the Agulhas already has substantial westward momentum when it reaches the tip, and the energy of the boundary region leaks more easily into the Atlantic than in E10. The great simplification of the bottom layer flow pattern (Fig. 12b) is particularly suggestive of this tendency. The only region with significant mean transport is un-

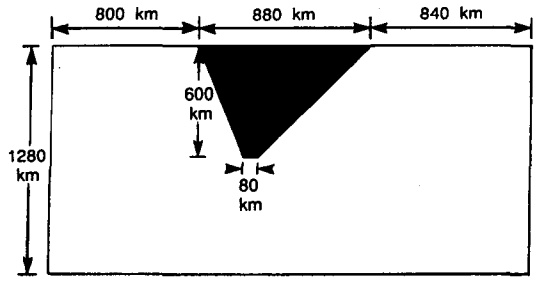

FIG. 11. Geometry of the ocean basin used in E11.

derneath the retroflection, which has even more variability than in E10. However, even this bottom circulation does not have the intensity it has in E10 (Fig. 13b in BD). The transport lines representing 15 and 20 Sv extend farther west but the 25 and 30 Sv lines are absent, as well as all those associated with other small circulations in the bottom layer of E10.

Another difference between E10 and E11 is the character of the stationary Rossby wave pattern in the Agulhas Return Current. Observations, described for instance by Harris and Bang (1974), indicate such a pattern in the Return Current. It is commonly attributed to conservation of potential vorticity as the current passes over bottom topographic features such as the Agulhas Plateau and the southern extensions of the Mozambique and Madagascar ridges. But in our flat bottom model, the existence of such waves must be derived from the necessity to increase the flow path through which the excess shear vorticity gained within the inertial–frictional coastal boundary layer can be diffused in order for the fluid to eventually rejoin a Sverdrup interior (Moore, 1963). According to Lutjeharms' (1980) statistical compilation of the dimensions of features in the retroflection region, the longer wavelength in E11 (~450 km) is more realistic than that in E10. The amplitude of the wave just east of the retroflection is also smaller. Thus, the aforementioned flow path is shorter, apparently because the boundary current picks up less relative vorticity along the sloping African coast.

That this latter assertion is true is supported by the observation in Fig. 13a that the current core gradually moves offshore as the tip of the Bank is approached, resulting in weaker shear on the coastal side of the current. A few hundred kilometers upstream from the tip, the core is next to the coast. Near the tip, the core is 90–100 km offshore. South of the tip, the mean Agulhas then branches, with 5–10 Sv turning into the Atlantic and about 20 Sv retroflecting into the Indian Ocean. The horizontal shear in the retroflecting branch is greatly reduced compared with E10, likely accounting for the shorter path required downstream for the fluid to return to an essentially Sverdrup interior, as suggested in the layer-1 mean flow patterns (comparing Figs. 13a of BD and 12a here).

b. E11 retroflection vorticity balance

It was mentioned in section 5a that a similarity of the E11 retroflection to that of NLIN1, E1 and E2 is in the almost always evolving character of the flow pattern, as rings form and drift toward the Atlantic (see Chassignet and Boudra, 1988). Unlike that of E3, E8 and E10, then, the retroflection vorticity balance of E11 must be viewed as that in which the major features of the retroflection are continually changing shape rather than as that associated with a quasi-steady configuration, subject to energetic fluctuations but only rare major disruptions. The signatures of ring formation in the mean mass and motion fields (Fig. 13a) are the branching into the Atlantic of a portion of the mean Agulhas and the relatively weak layer thickness gradient directly west and then northwest from the western edge of the retroflection.

The most interesting new aspect of the E11 retroflection is the aforementioned offshore displacement of the current core as the tip of Africa is approached. The terms of the mean vorticity balance have values of the same order as the maxima in E3 and E10 only in the coastal Agulhas, and especially where the core is no longer attached to the coast. Since the return current is more zonal and less nonlinear, BETA, STRCH and RVA are all relatively small downstream of the eastward turn. Even along the coast, BETA (Fig. 13b) is smaller, since only 70% of the velocity magnitude is in the southward component.

A major portion of the positive vorticity generation along the coast is in STRCH. The coastal band of

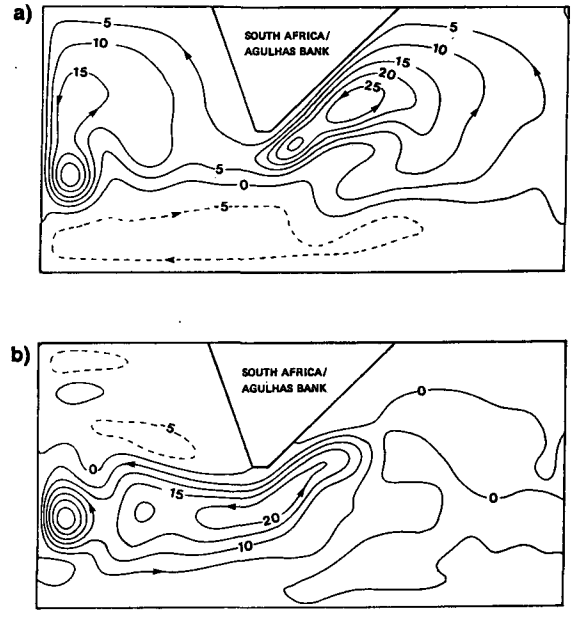

FIG. 12. Experiment E11. (a) Upper layer mean mass transport streamfunction for the last half of the 3650 day experiment. The contour interval is 5 Sv. (b) As (a) for layer 3.

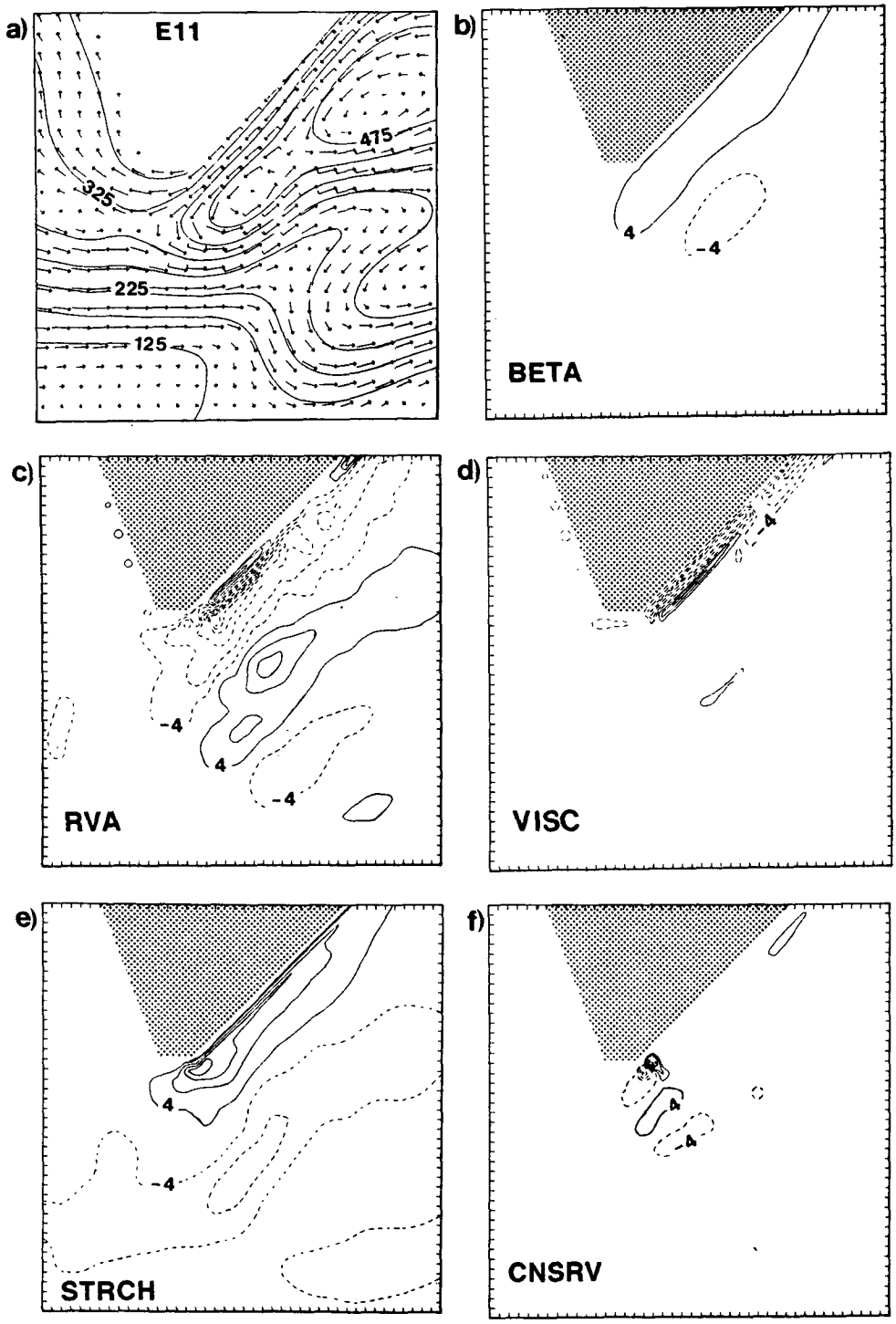

FIG. 13. As in Fig. 9 for Experiment E11.

STRCH, broadening toward the southwest, is understood in terms of the mass/flow field geostrophic balance as the core moves away from the coast. The displacement is associated, by the thermal wind relation, with the lifting of the isopycnal layer interface between the current core and the coast. This is evident in the increasing distance of the 325 and 375 db thickness contours from the coast as the tip of the Bank is approached (Fig. 13a). A similar but smaller displacement of the same contours from the coast is seen in Fig. 9a

for E10, although not associated with offshore motion of the current core. We will return to this lifting of the isopycnal interface and its role in the model retroflection in the concluding section of the paper. The positive vorticity generation where the mean current is turning back toward the Indian Ocean is contributed by approximately equal components of STRCH and BETA, suggesting that both are important in the actual retroflection.

On the coastal side of the current core, a new structure appears in VISC (Fig. 13d), mainly where the core has moved significantly offshore. The latter gives the grid an opportunity to resolve the inshore side of the current, and, as well as generation of negative vorticity along the first row of grid points from the no-slip boundary, a band of positive generation is noted along the second row. As VISC changes sign, RVA does so, also, to balance it. In E10, the current is only so well-resolved after separation, so that the positive features appear only south of Africa's tip. This brings attention again to the fact that 20 km resolution inadequately describes the details of boundary layer flows. Notably, the positive feature just south of Africa's tip, seen in the vorticity balances of LIN2, NLIN1, E1, E3 and E10 is absent. This is due to the fact that the mean Agulhas does not separate from the coast in E11, as it does in those experiments, but has a branch remaining attached to the coast as it rounds the tip. Separation is required for this positive feature to be resolved by the grid.

CNSRV (Fig. 13f) is even less important than in E10, as only two grid points at Africa's tip have values on the same order as the other terms. In this high resolution experiment, therefore, the basic finite difference expressions of BETA, RVA and STRCH have little difficulty conserving potential vorticity and potential enstrophy.

7. Summary

The vorticity balance has been used as a tool with which to describe and understand the dynamics of Agulhas Current retroflection in an idealized numerical model of the South Atlantic–Indian Ocean. First, the numerical model and experimental design were summarized. The vorticity equation was then developed from the model equations of motion, and the equilibrium vorticity balance was stated to be among wind stress curl (WIND), viscous stress curl (VISC), planetary (BETA) and relative (RVA) vorticity advection, stretching (STRCH) and extra terms deriving from the requirement that the nonlinear terms of the numerical model, like those in the exact differential equations, conserve potential vorticity and potential enstrophy (CNSRV). It was recognized that the contribution of CNSRV to the balance should diminish as horizontal resolution is improved. In experiments reaching a steady state, the balance was computed for the steady conditions. For experiments reaching only statistical equilibrium, the balance was computed for the last half of a 3650 day integration.

A demonstration with a 1000 m thick one-layer simplification of the Bleck and Boudra (1981) model, on a basin in which Africa is represented as a rectangle extending from the northern boundary, showed that either strong internal friction or inertia can bring about a partial retroflection where a linear model with weak friction has none. In the first case, BETA is balanced by VISC for some distance south of Africa, allowing Agulhas streamlines to reach eastward directed Sverdrup lines to the south—in essence, retroflection through a broadening of the frictional boundary layer. In the case with inertia and strong friction, only the orientation of retroflection changes, and BETA is still balanced primarily by VISC. It was pointed out that Agulhas retroflection in coarse resolution ocean general circulation models is likely of this frictionally dominated type. With weak friction much of the current actually turns eastward in response to BETA, balanced now by RVA. After making this turn, the fluid drifts eastward or southeastward through a stationary Rossby wave pattern, finally attaching to the streamlines of the linear solution. In this case, the retroflection is accomplished within a free boundary layer as suggested by de Ruijter (1982). But the mechanism differs from his "inertial overshooting distance."

Stratification was introduced, using now the Bleck and Boudra (1981) quasi-isopycnic coordinate model with weak friction, first in a relatively low Rossby number, 2-layer experiment with 1000 m mean upper layer thickness. In the multilayer experiments, only the vorticity balance in the top layer, the one containing virtually all of the linear wind-driven transport, is computed. Along the rectangular Africa's east coast, the vorticity balance was shown to be almost identical to that in the weakly frictional one-layer model: between BETA and VISC next to the coast and between BETA and RVA on the seaward side of the current core. The stretching term, identically zero in the one-layer rigid lid model, however, was found to complement BETA in the region south of Africa, resulting in a reduction in the latitudinal scale of the retroflection with respect to the one-layer case. By making a substitution from the model mass continuity equation, it was shown that, for equilibrium conditions, the stretching term is proportional to the mean value of the product of layer thickness advection and the inverse of layer thickness. In contrast to one layer and quasi-geostrophic models, this highly nonlinear term becomes important in the vorticity balance of stratified primitive equation models when isopycnals vary substantially from the horizontal.

It was shown that when the Rossby number/baroclinicity is increased by adding more stratification and reducing mean top layer thickness, the importance of the stretching term correspondingly increases, con-

tinuing to complement BETA, but with double or triple its magnitude. The retroflection is thus strengthened, and, with 300 m top layer thickness, almost 100% of the Agulhas reaching Africa's tip retroflects. In this case, the isopycnal layer thickness variation is the same order as the total layer-1 thickness.

When grid-point spacing is reduced from 40 to 20 km, the western boundary layers and baroclinic instability are better resolved. This results in further strengthening of the mean retroflection, accompanied by a slight weakening of the retroflection eddy intensity. Mostly minor changes in the retroflection vorticity balance are noted, but an important reduction in the role of CNSRV, the sum of extra terms resulting from the model's built-in conservative properties, is obtained. With 40 km resolution and 300 m top layer thickness, CNSRV was shown to be essential in the retroflection strength. With resolution of 20 km, CNSRV has values on the same order as BETA, RVA, VISC and STRCH only very close to separation, suggesting that it no longer plays such an important role in the retroflection. That its importance diminishes suggests that BETA, RVA and STRCH are more potential enstrophy conserving in their own right. This trend is consistent with the notion that, as grid point spacing is decreased, basic finite difference expressions of the partial derivatives more accurately represent those derivatives, and the characteristics of the numerical model solution more closely approximate those of the exact solution.

The importance of the frictional boundary condition on Africa was brought out through a no-slip/free-slip comparison. It was shown that a large negative value of VISC on the coastal side of the boundary current is needed in order for it to separate easily at the tip. Such a current is one which is already substantially sheared on its coastal side before separation, which the no-slip condition implies, so that it flows easily into an open ocean.

Finally, the β-effect in the separating Agulhas was put in a more realistic perspective by introducing a new South African Geometry actually approximating the shape of the Agulhas Bank shelf break, along which the real Agulhas flows after leaving the coast of South Africa. In this geometry, approximately 70% of the Agulhas velocity magnitude is advecting planetary vorticity, as opposed to 100% with the meridionally oriented coast. In an experiment otherwise similar to the previous high resolution case with rectangular geometry, it was found that the retroflection is still relatively strong though the mean circulation near Africa's tip is considerably weaker. In the upper layer, now 5 to 10 Sv of Southwest Indian Ocean water flows into the South Atlantic in the mean, principally within Agulhas rings, which form along the sloping coast near Africa's tip and drift into the Atlantic at the rate of 2 to 3 per 365-day period (see Chassignet and Boudra, 1988). The change in coastal orientation at Africa's tip is not as abrupt as in the previous configuration, and the mean current does not separate from the coast there. Instead, a branch on the coastal side of the core remains attached to the coast as it turns into the Atlantic and the other branch, representing the major portion of the Agulhas, turns back into the Indian Ocean over a broad region south and southeast of the tip.

An interesting new aspect of the retroflection using more realistic geometry is the separation of the mean current core from the coast several hundred kilometers upstream from the tip. As it begins to turn back eastward, the core is running parallel to the coast, 90–100 km offshore. Associated with this offshore displacement of the core is a lifting of the first isopycnal layer interface on its coastal side as the tip is approached. The value of BETA is substantially reduced, as well as its importance in the vorticity balance along the coast. The major component of the balance contributing positive vorticity here is STRCH, which is directly related to the lifting of the layer interface. As in the previous cases, viscous effects are strong between the current core and the coast and are balanced now primarily by stretching and relative vorticity advection. Where the large part of the current is turning back toward the Indian Ocean the magnitude of STRCH is reduced. Here BETA and STRCH contribute approximately equal amounts of positive vorticity, suggesting that both are important in the retroflection. Also, the broader current picks up less negative relative vorticity along the coast and is less nonlinear as the major portion turns eastward than in the previous multi-layer experiments. The fluid path in the Agulhas Return Current is, therefore, more zonal and the terms of the vorticity balance much smaller than with the rectangular Africa.

8. Discussion

The analysis presented here confirms the hypothesis advanced by de Ruijter and Boudra (1985) and Boudra and de Ruijter (1986): that the model Agulhas retroflection results from the change in the vorticity balance as the current leaves the South African coast for the open ocean. It is apparent, first of all, that a strongly frictional boundary condition is required for the current to separate when inertia is strong enough to overcome the linear tendency to make the sharp westward turn. Along such a coast, the friction provides a sink for the β-induced gain of positive vorticity. As the current separates, friction diminishes and, in the one layer model, the continued β-generation of positive vorticity results in the eastward turn. As the vertical structure becomes more baroclinic in the multilayer model, positive vorticity is induced by both β and the mean divergent component of flow through the stretching term. Again, once the dissipative sink of this positive vorticity has

been left behind, the fluid expresses the gain of vorticity in a counterclockwise turn.

It is natural to ask why the stretching term acts in the same sense as β so that the retroflection becomes stronger so rapidly as the top layer thickness is decreased. This may be explained if we remember that the equilibrium stretching term is proportional to the temporal mean of layer thickness advection times the inverse of layer thickness, and consider the large scale deformation of the first layer interface, which is set up by the basin structure and wind-forcing pattern. This way of looking at the stretching term suggests that wherever fluid parcels move from large toward small layer thickness, positive relative vorticity will be induced. In this respect, the term acts like a planetary or topographic β. Though not rigid, like lines of constant f and bottom depth, the isopycnals' large scale structure may be considered quasi-steady once equilibrium conditions have been reached. In the retroflection region of our model, the isopycnal layer interface slopes upward toward the subpolar gyre and toward the eastern subtropical Atlantic. In the mean, then, motions toward the south or west out of the retroflection tend to generate positive relative vorticity, encouraging the fluid to return. Conversely, northward motion on the east side of the retroflection eddy is generally toward larger layer thickness and generates negative relative vorticity, resulting in cyclonic curvature out of the retroflection toward the east. The planetary β-effect and the stretching term thus complement each other.

At this point, it is instructive to consider some similarities and differences with the Ou and de Ruijter (1986) model. Their model contains two of the elements which are of primary importance in our model retroflection: inertia and β. It does not include coastal friction (which is of utmost importance in our model), temporal variability, or motion in more than one layer. Both models, however, apparently achieve boundary current separation with a motionless condition on the west (or northwest) side of the current—in their case, as the motionless lower layer outcrops along the coast, in ours through use of a highly frictional boundary condition. In fact, separation in our model usually occurs as the current shoots past a very abrupt change in the boundary orientation.

In the final experiment here, the change in coastal orientation is less abrupt. In fact, the shape lacks their convex curvature, but is otherwise quite similar to the one with which Ou and de Ruijter obtain retroflection. Correspondingly, the similarity between the mean retroflection flow pattern in our experiment and their calculated path for the Agulhas greatly increases. In particular, the core of the model Agulhas separates from the coast at approximately the same upstream distance from the southern tip as their Agulhas separates, and begins retroflecting as it is passing the tip, also like their current. The physical mechanism of the layer interface outcrop in their model is the positive shear vorticity induced by β, which through the thermal wind relation, must be accompanied by increased isopycnal interface tilt. At some distance down the coast, then, the interface reaches the upper surface at the coast, and the current must separate. The first isopycnal layer interface in our model does not outcrop, but it does rise along the coast as the current core separates. While their model is much simpler than ours, the similarity between our mean flow pattern and their current path suggests that the same physical mechanism may be at work.

From their one and one-half layer model calculations, Ou and de Ruijter (1986) conclude that inertia and β together play a dominant role in the retroflection. After investigating the details of our numerical model retroflection, we would add to this list coastal friction, which acts as a sink of some of the β-induced gain of positive vorticity. In addition, a major finding of this study with a fully baroclinic model concerns the importance of the upper ocean distribution of water masses, which is set up in reality by both wind and thermohaline forcing. Our model results suggest that low magnitude potential vorticity waters of the southwest Indian Ocean, attempting to escape westward south of Africa's tip into the higher magnitude potential vorticity waters of the eastern subtropical South Atlantic, experience a torque, through the stretching term of the vorticity equation, which helps to drive them back toward the Indian subtropical gyre.

Acknowledgments. We wish to acknowledge many helpful discussions with Prof. Claes Rooth, Prof. Rainer Bleck, and Ms. Linda Smith. This work has been supported by the Office of Naval Research Contract No. N00014-85-C0020. Computations were performed using the Cray-1 computers at the National Center for Atmospheric Research, which is sponsored by the National Science Foundation.

REFERENCES

Bleck, R., 1979: Finite-difference equations in generalized vertical coordinates. Part II: Potential vorticity conservation. *Contrib. Atmos. Phys.*, **51**, 360–372.

——, and D. B. Boudra, 1981: Initial testing of a numerical ocean circulation model using a Hybrid (quasi-Isopycnic) vertical coordinate. *J. Phys. Oceanogr.*, **11**, 755–770.

Boudra, D. B., and W. de Ruijter, 1986: The wind-driven circulation in the South Atlantic-Indian Ocean. II. Experiments using a multi-layer numerical model. *Deep-Sea Res.*, **33**, 447–482.

Chassignet, E. P. and D. B. Boudra, 1988: Dynamics of Agulas retroflection and ring formation in a numerical model II: Energetics and ring formation. *J. Phys. Oceanogr.* **18**, 304–319.

Bryan, K., 1963: A numerical investigation of a nonlinear model of a wind-driven ocean. *J. Atmos. Sci.*, **20**, 594–606.

Darbyshire, J., 1972: The effect of bottom topography on the Agulhas Current. *Rev. Pure Appl. Geophys.*, **101**, 208–220.

De Ruijter, W., 1982: Asymptotic analysis of the Agulhas and Brazil Current system. *J. Phys. Oceanogr.*, **12**, 361–373.

——, and D.B. Boudra, 1985: The wind-driven circulation in the South Atlantic–Indian Ocean. I. Numerical experiments in a one-layer model. *Deep-Sea Res.*, **32,** 557–574.

Harris, T. F. W., and N.D. Bang, 1974: Topographic Rossby waves in the Agulhas Current. *S. Afr. J. Sci.*, **70,** 212–214.

Hellerman, S., and M. Rosenstein, 1983: Normal monthly wind stress over the world ocean with error estimates. *J. Phys. Oceanogr.*, **13,** 1093–1104.

Holland, W. R., and L. B. Lin, 1975: On the generation of mesoscale eddies and their contribution to the oceanic general circulation. I. A preliminary numerical experiment. *J. Phys. Oceanogr.*, **5,** 642–669.

Lutjeharms, J. R. E., 1981: Spatial scales and intensities of circulation of the ocean areas adjacent to South Africa. *Deep-Sea Res.*, **28A,** 1289–1302.

——, and R. C. van Ballegooyen, 1984: Topographic control in the Agulhas Current System. *Deep-Sea Res.*, **31,** 1321–1337.

——, and A. Gordon, 1987: Shedding of an Agulhas ring observed at sea. *Nature*, **325,** 138–140.

Moore, D. W., 1963: Rossby waves in ocean circulation. *Deep-Sea Res.*, **10,** 735–747.

Niiler, P. P. and A. R. Robinson, 1967: The theory of free inertial jets. II. A numerical experiment for the path of the Gulf Stream. *Tellus*, **19,** 601–619.

Olson, D. B., and R. H. Evans, 1986: Rings of the Agulhas. *Deep-Sea Res.*, **33,** 27–42.

Ou, H. W., and W. de Ruijter, 1986: Separation of an inertial boundary current from a irregular coastline. *J. Phys. Oceanogr.*, **16,** 280–289.

Warren, B. A., 1963: Topographic influences on the path of the Gulf Stream. *Tellus*, **15,** 167–183.